http://ansinet.com/itj

ITJ

ISSN 1812-5638

INFORMATION TECHNOLOGY JOURNAL

ANSInet
Asian Network for Scientific Information
308 Lasani Town, Sargodha Road, Faisalabad - Pakistan

Information Technology Journal 8 (8): 1094-1114, 2009
ISSN 1812-5638

Characteristics of Flow past a Square Cylinder using the Lattice Boltzmann Method

S. Ul-Islam and C.Y. Zhou
Harbin Institute of Technology, Shenzhen Graduate School, Shenzhen University Town,
Shenzhen 518055, China

Abstract: The Lattice Boltzmann Method (LBM) has been seen as an alternative tool for the computational simulation of fluid dynamics. In this study, we use the LBM with Single-Relaxation-Time (SRT) collision model to simulate two-dimensional (2D) laminar flow past a square cylinder. The main aim of the study is to systematically investigate the influences of the locations of the inflow, outflow and side walls boundaries, where Reynolds number is kept at 100 for all calculations. The side wall boundary locations will be analyzed using the periodic and symmetric boundary conditions. Analyses of the relaxation time parameter also have been investigated. Some physical quantities, such as the drag coefficient, mean drag coefficient, root mean square values of lift coefficient and the Strouhal number are examined for the purpose. We also examined the vortex shedding formation which provides an excellent means of visualizing the von Karman vortex street. We found that there is a certain range for inflow, outflow and side wall boundaries where physical quantities such as drag and mean drag coefficients, root mean square value of lift coefficient and the Strouhal number show some changes. Results also show that, there is a change for physical quantities when the relaxation time parameter is changed from certain range and also effect the computational time. The physical quantities are obtained and compared with other existing experimental and numerical results.

Key words: Lattice Boltzmann method, single relaxation time, square cylinder, vortex shedding, mean drag coefficient, Strouhal number

INTRODUCTION

Flow around a square cylinder is of practical importance in many fields of engineering and science. Now, practical applications are easily found in the form of flow around tall buildings and bridges etc. There have been numerous detailed studies of flow past a square cylinder. The motivation for the preset study has been taken into account after studying the following available literature.

The open literatures are very limited for flow past a square cylinder. The flow patterns such as vortex shedding behind a rectangular cylinder have been investigated both numerically and experimentally by several authors. Davis and Moore (1982) reported numerical results generated by their SIMPLEC code. Davis *et al*. (1984) examined confined flow past a rectangular cylinder both numerically and experimentally. Franke *et al*. (1990) examined numerical results for Reynolds number less than or equal to 300 using the SIMPLEC code. Sohankar *et al*. (1996) examined quite different numerical methods for two-dimensional and three-dimensional unsteady flows around a square cylinder and observed that a transition from 2 to 3D shedding flow may occur for Reynolds number between 150 and 200. Okajima (1982) carried out an experiment using a water tank. Okajima provided results from multiple experiments at each tested Reynolds number within the range 80 and 150. Shimizu and Tanida (1978) experimentally studied the effect of fluid forces on cylinders of rectangular cross section.

The selection of the upstream, downstream and side wall locations are very important as it affects the quality of the solution. Too small a computational domain distorts the alternating vortices and also affects the size and width of the vortices. However, choice of a larger computational domain requires more grid points that leads to increase in computational time. Thus, selection of the computational domain is crucial. There have been few systematic studies to measure these types of problems. Sohankar *et al*. (1998) carried out the second-order Crank-Nicolson study of the flow past a square cylinder and provide some physical

Corresponding Author: C.Y. Zhou, Harbin Institute of Technology, Shenzhen Graduate School, Shenzhen University Town, Shenzhen 518055, China Tel: 0086-755-25961297 Fax: 0086-755-26033774

analysis and explanations of physical quantities like drag coefficient and Strouhal numbers etc. of their numerical results for the influence of upstream, downstream and side wall positions. There results show how to reduce the CPU time by reducing the upstream influence from the outlet and then reducing the necessary downstream. They also investigated the blockage effect of walls and side ratios for the square cylinder. Their simulations were carried out for two-dimensional flows at low Reynolds numbers (R_e). They further reported that if the blockage is reduced from H = 20 to H = 40, the maximum change in mean drag coefficient ($<C_d>$), root mean square value of lift coefficient (C_{lrms}) and Strouhal number (S)$_t$ is 1.4%. Recently, Hassan *et al*. (2005) examined the outflow boundary around a circular and a square cylinder using the Physical Boundary Conditions (PBC) for fairly low R_e. Their results show that the PBC enhanced the computational efficiency for such type of flows for more truncated domain. They fully investigated the influence on physical quantities such as mean drag coefficient, peak value of lift coefficient and Strouhal number for different outflow boundary locations.

We focused our attention to systematically investigate the above mentioned problems using the LBM. The accuracy of LBM strongly depends on the relaxation time parameter τ. Recently, Kruger *et al*. (2009) examined the influence of relaxation time parameter τ for the case of a poiseuille flow through a rectangular channel in three dimensions. They examined that relaxation time parameter τ have a strong influence on the accuracy of the simulations. They recommend the relaxation time parameter $\tau \approx 0.9$ for such type of flows. There is a very detailed analysis of the lattice Boltzmann error in (Hollis *et al*., 2006) and the choice of relaxation time parameter τ (Latt and Chopard, 2008). We also examined the affect of relaxation time parameter for flow past a square cylinder in detail in present study.

We examined the wall boundary locations using quite different boundary conditions, such as periodic and symmetric boundary conditions. The motivation for such types of side boundary conditions has been taken into account after studying the following literature. Fornberg (1991) proposed quite different numerical methods to examine the physical quantities such as drag coefficient for the flow past a row of circular cylinders at large Reynolds number. He examined the transition from small blockage ratio β = w[R] (where R is the radius of the circular cylinder) to high blockage ratios and find the critical range $\beta \approx 8$. Ingham *et al*. (1990) examined the same flow problem for a row of normal flat plates using quite different numerical methods.

The main objectives of the present study were to further investigate such types of problems using the LBM.

LATTICE BOLTZMANN METHOD

The Lattice Boltzmann Method (LBM) is a mesoscopic method (He and Luo, 1997a; Chen *et al*., 1992). Historically, it has been originated from Cellular Automata (CA) models (Frisch *et al*., 1986; Wolfram, 1986). He and Luo (1997b) examined that LBM can be considered as a special discrete form of the continuous Boltzmann equation. In LBM, a single particle distribution function, $f_i(x, t)$, representing the number of particles at site x moving in direction e_i at time t. Each group of particles can move only in a finite number of directions on a discrete lattice shown in Fig. 1. Therefore, the physical and velocity space are discretized into a regular lattice and a finite set velocities (e_i), respectively (Qian *et al*., 1992). The macroscopic density, ρ and velocity, u, can be obtained in the following way from the distribution function:

$$\rho = \sum_{i=0}^{\infty} f_i \tag{1}$$

and

$$u = \frac{1}{\rho}\sum_{i=1}^{\infty} f_i e_i \tag{2}$$

The single particle distribution function, $f_i(x, t)$, on each site during the time space, Δt, on a discrete lattice is modified according to collisions. This change is given by the following evolution equation:

$$f_i(x + e_i\Delta t, t + \Delta t) = f_i(x,t) + \Omega_i \tag{3}$$

where, Ω_i is the collision operator. The collision operator must need to maintain the total mass and momentum (and energy in isothermal problems).

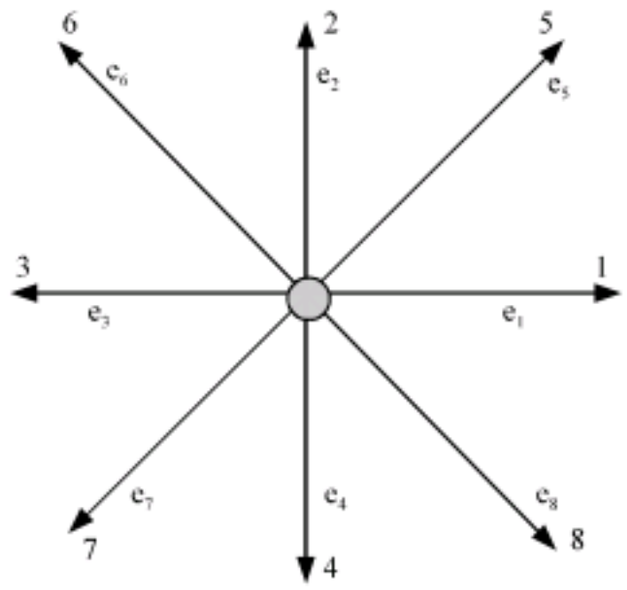

Fig. 1: A Two-dimensional nine-velocity lattice (D2Q9) model

Bhatnagar *et al*. (1954) described a collision operator to consider the collision effects between particles. As a relaxation process to the local equilibrium state the collision process describes in the following way:

$$\Omega_i = -\frac{\Delta t}{\tau}\left[f_i - f_i^{(eq)}\right] \quad (4)$$

where, τ is the non-dimensional relaxation time and $f_i^{(eq)}$ is the single particle local equilibrium distribution.

A careful selection of τ is very important in Lattice Boltzmann (LB) modeling, because the numerical stability of LB modeling depend on the value of τ. The governing mesoscopic single-relaxation-time BGK equation (Bhatnagar *et al*., 1954) for the LBM will be:

$$f_i(x + e_i\Delta t, t + \Delta t) = f_i(x,t) - \frac{\Delta t}{\tau}\left[f_i - f_i^{(eq)}\right] \quad (i = 0,1,2,...,8) \quad (5)$$

After the collision step, the streaming step requires to be transmitted the local information at each node to its neighbor site $x+e_i\Delta t$ at time $t+\Delta t$. The equilibrium distributions play an important rule to recover the macroscopic dynamics of fluids by Navier-Stokes (NS) equations. The chosen equilibrium distribution functions (Qian *et al*., 1992) are defined as:

$$f_i^{(eq)} = \alpha_i\rho\left[1 + \frac{3}{c^2}(e_i.u) + \frac{9}{2c^4}(e_i.u) - \frac{3}{2c^2}|u|^2\right] \quad (i = 0,1,2,...,8) \quad (6)$$

where, α_i are the weighting factors to ensure isotropy and C is the lattice speed. Equation 6 shows a better approximation for low Mach Numbers. The values of α_i for two-dimensional model are tabulated in Table 1.

The macroscopic equations can be obtained by a multiscale method such as Chapman (1970) to ensure that the system describe above recovers the incompressible regime for the following governing equations:

$$\nabla.u = 0 \quad (7)$$

$$\frac{\partial u}{\partial t} + u.\nabla u = -\frac{\nabla p}{\rho} + \upsilon\nabla^2 u \quad (8)$$

The thermodynamic pressure, p and kinematic viscosity, ν, can be obtained in the following way:

$$p = \rho c_s^2 \quad (9)$$

$$\nu = c_s^2\left(\tau - \frac{1}{2}\right)\frac{h^2}{\Delta t} \quad (10)$$

Table 1: Parameters for the lattices D2Q9

Lattice	D2Q9
α_0	4/9
$\alpha_{1,2,3,4}$	1/9
$\alpha_{5,6,7,8}$	1/36

The corresponding velocities $|e_0| = 0, |e_{i=1,2,3,4}| = 1, |e_{i=5,6,7,8}| = \sqrt{2}$ corresponds to weighting factors α_0, $\alpha_{i=1,2,3,4}$ and $\alpha_{i=5,6,7,8}$, respectively

where, h is the lattice spacing. It is clear from Eq. 10 that the dimensionless relaxation time related to the kinematic viscosity ν of the fluid and the speed of sound C_s. The relation between fluid speed of sound C_s and the lattice speed C is $c_s = \frac{c}{\sqrt{3}}$.

Simulation parameters play an important rule in LB modeling. To ensure the incompressible regime the computational Mach number (M_a) must need to satisfy the following condition:

$$M_a = \frac{U_{max}}{C} << 1 \quad (11)$$

where, U_{max} is the maximum simulated fluid velocity.

PROBLEM DESCRIPTION

The geometry of computational domain for flow past a square cylinder placed in a channel as shown in Fig. 2. A square cylinder placed in the middle of the channel to examine all the issues earlier.

Initial condition: The following procedure is incorporated as an initial condition:

$$u = v = 0 \quad (12)$$

and

$$\rho = \rho_0 \quad (13)$$

Inlet and outlet boundary conditions: Uniform flow is incorporated using the equilibrium particle distribution function at the inlet in the following way:

$$f_i = f_i^{(eq)}(U_{max}) \quad (14)$$

where, U_{max} is the maximum inflow velocity. At the outflow boundary, due to extremely large domain behind the cylinder, from the results no influence is expected and a fixed pressure is imposed in terms of the equilibrium distribution function at the outlet Succi (2001).

Side wall boundary condition: To examine the influence of relaxation time parameter τ, upstream and downstream boundary locations we adopted the bounce-back

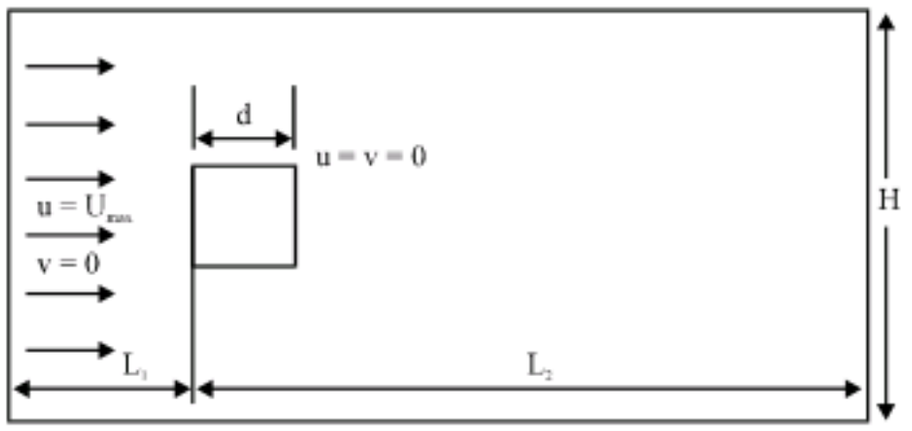

Fig. 2: Simulation domain for the fluid flow with built in square cylinder in a channel. L_1, inlet position of the cylinder, L_2 outlet position of the cylinder, H, height of the computational domain and d, diameter of the cylinder

boundary conditions on the walls (Wolf-Gladrow, 2000). Bounce-back boundary condition is the reversion of particles momentum, in which all particles hitting the wall and reflected back to its previous position (this is a way or a treatment that to fulfill the boundary condition of non-slip condition), i.e.,

$$f_{-i}(x,t+1) = f_i(x,t_+) \tag{15}$$

where, −i denotes the opposite direction of i.

Boundary conditions for side wall locations: The periodic and symmetric boundary conditions are adopted to investigate the side wall locations.

Symmetric boundary condition: The boundary conditions at j = 1 for the particle distribution function are given by the following way:

$$\begin{aligned} &f_0(i,1) = f_0(i,3), f_1(i,1) = f_1(i,3), f_2(i,1) = f_4(i,3),\\ &f_3(i,1) = f_3(i,3), f_4(i,1) = f_2(i,3), f_5(i,1) = f_8(i,3),\\ &f_6(i,1) = f_7(i,3), f_7(i,1) = f_6(i,3), f_8(i,1) = f_5(i,3) \end{aligned} \tag{16}$$

Similar condition adopted for j = NY.

Periodic boundary condition: In such type of boundary condition the on boundary (neighboring) point is located on opposite boundary and implemented by the following way:

$$\begin{aligned} ip &= (i < NX-1)(i+1) : (0)\\ in &= (i > 0)(i-1) : (NX-1)\\ jp &= (j < NY-1)(j+1) : (0)\\ jn &= (j > 0)(j-1) : (NY-1) \end{aligned} \tag{17}$$

where, ip, in, jp and jn are integers and located on opposite boundary node. The two indexes i and j represents the looping for transverse and lateral directions, respectively (Sukop and Thorne, 2007).

Surface of the object: The surface of the cylinder was defined with a no slip wall boundary condition and this is realized with a bounce-back boundary treatment. No-slip condition ensures that the fluid will have zero velocity relative to the boundary.

Force evaluation: The momentum exchange method (Dazhi *et al*., 2003) was used in the present study for simulating flow around square cylinder. The total resultant fluid force, F, on a fixed solid body is obtained in the following way:

$$F = \sum_{all\ X_b} \sum_{\alpha=1}^{N} e_\beta \left[n_\alpha(X_b,t) + n_\alpha\left(X_b + e_\beta \delta t, t\right) \right] \frac{\delta x}{\delta t} \tag{18}$$

where, N is the non-zero lattice velocity vectors, the subscript α is the opposite lattice direction of β, i.e., α = −β = 1, 2,...,8.

To obtain the fluid solid momentum exchange per unit time Eq. 8 is treated at the midpoint for the fluid lattice node $x_f = (x_b+e_\beta\delta t, t)$ and the solid lattice node $x_b = (x_f+e_\alpha\delta t, t)$. Where x_b denotes the solid nodes and x_f represents the fluid nodes. The distribution function used as a post collision state. The momentum exchange between a solid node at x_b and all possible neighboring fluid nodes around that solid node can be obtained by the inner summation. While the force contribution for all boundary nodes at x_b given by the outer summation.

The Reynolds number is a measure of the ratio of maximum velocity, U_{max}, diameter of the cylinder, d and kinematic viscosity of fluid, ν, is:

$$R_e = \frac{U_{max} d}{\nu} \tag{19}$$

The non-dimensional frequency of vortex shedding refers as Strouhal number (S_t). Strouhal (1878) proposed such a dimensionless parameter, later on Benard (1926) called as Strouhal number. The frequency at which vortex shedding takes place can be desired using the following equation for fixed Reynolds numbers:

$$S_t = \frac{f_s d}{U_{max}} \tag{20}$$

where, S_t is the Strouhal number, f_s is the vortex shedding frequency.

The drag coefficient, C_d and lift coefficient, C_l, defined as:

Table 2: Computational domain for upstream locations

L_1 (d)	L_2 (d)	H (d)
1.5	35	10
3	35	10
6	35	10
9	35	10
15	35	10

Table 3: Computational domain for outlet boundary locations

L_1 (d)	L_2 (d)	H (d)
15	6	10
15	8	10
15	15	10
15	22	10
15	27	10
15	35	10

Table 4: Computational domain

R_e	$L_1 \times L_2$	H
100	1001	61
100	1001	101
100	1001	151
100	1001	201
100	1001	251
100	1001	301
100	1001	351
100	1001	401

$$C_d = \frac{F_x}{\frac{1}{2}\rho U_{max}^2}, \qquad C_l = \frac{F_y}{\frac{1}{2}\rho U_{max}^2} \tag{21}$$

where, ρ, F_x and F_y are density, drag and lift forces, respectively.

Fast Fourier Transform (FFT) technique adopted to obtain the frequency domain (Strouhal number) of the lift force time histories data. The FFT technique works best when the time interval Δt is equal (Bendat and Piersol, 1971).

The percentage error between two values can be finding using the following Eq. 22:

$$\text{Error } (\%) = \frac{\text{abs}(A - B)}{\text{abs}(B)} \times 100\% \tag{22}$$

where, A represent the present numerical data and B represent the chosen data from open literature.

The computational domains for different inflow locations are tabulated in Table 2.

For the simulation of outflow locations, L_1, L_2 and H are shown in Table 3.

The various computational domains for all side wall locations are shown in Table 4.

RESULTS AND DISCUSSION

Figure 3 shows the time histories of the lift coefficients for different single-relaxation-time parameters.

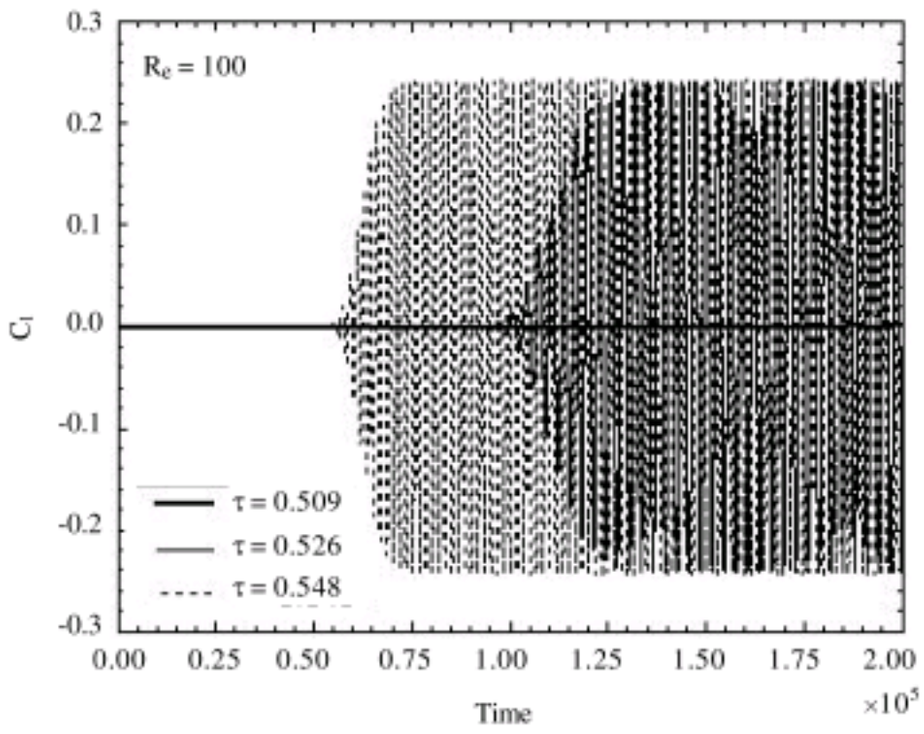

Fig. 3: Variation of lift coefficient with respect to time

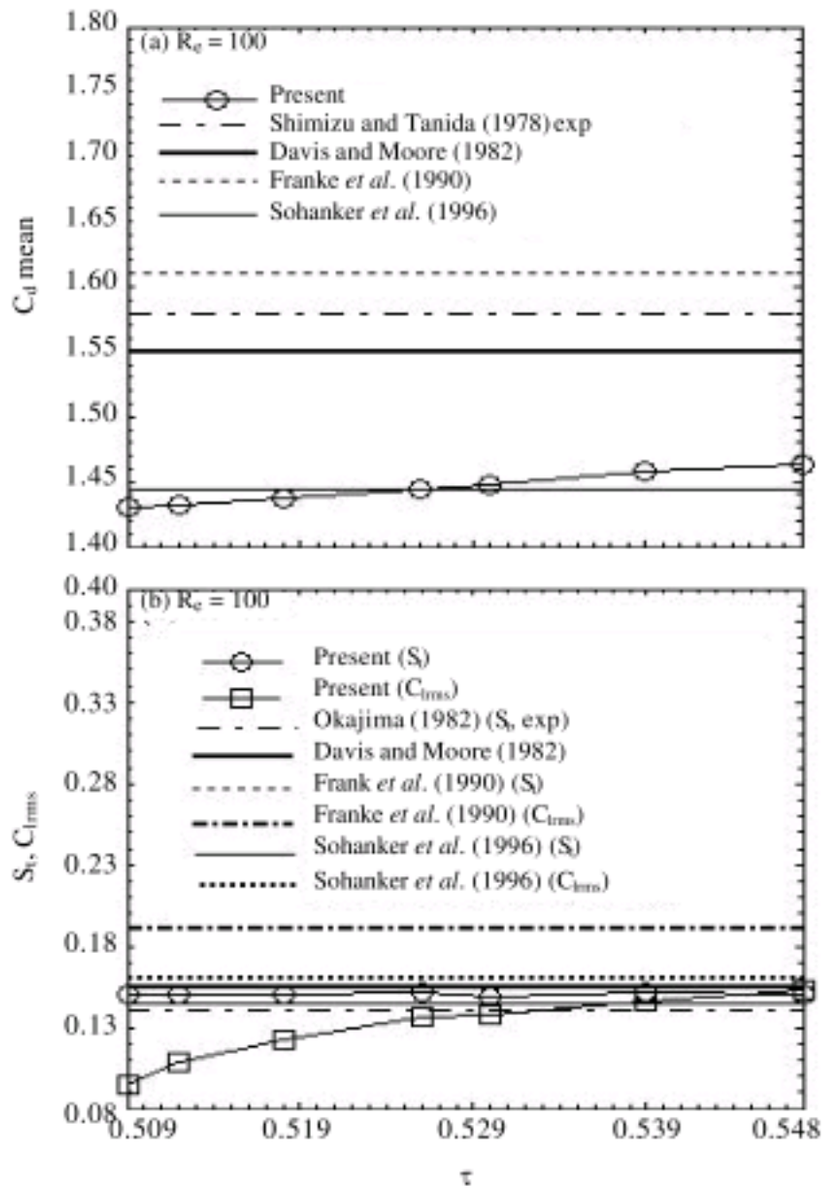

Fig. 4: (a) Comparison among mean drag coefficient and (b) Strouhal numbers and root mean square value of lift coefficient for flow past a square cylinder for different relaxation time parameters

In order to asses the influence of relaxation time parameter τ, we have computed mean drag coefficient, root mean square value of lift coefficient and Strouhal number for flow past a square cylinder and compared with the open literature data and plotted together in Fig. 4a and b.

Figure 5a-g show the patterns of vorticity contour lines for different single-relaxation-time parameter.

The Strouhal numbers obtained in the present study are given in Fig. 6a-c for different relaxation time parameter.

Figure 7a and b show the drag and lift coefficient history developments for $\tau = 0.548$.

In Fig. 8a and b, both the numerical and experimental data from open literature and values from this study are shown for different inflow locations.

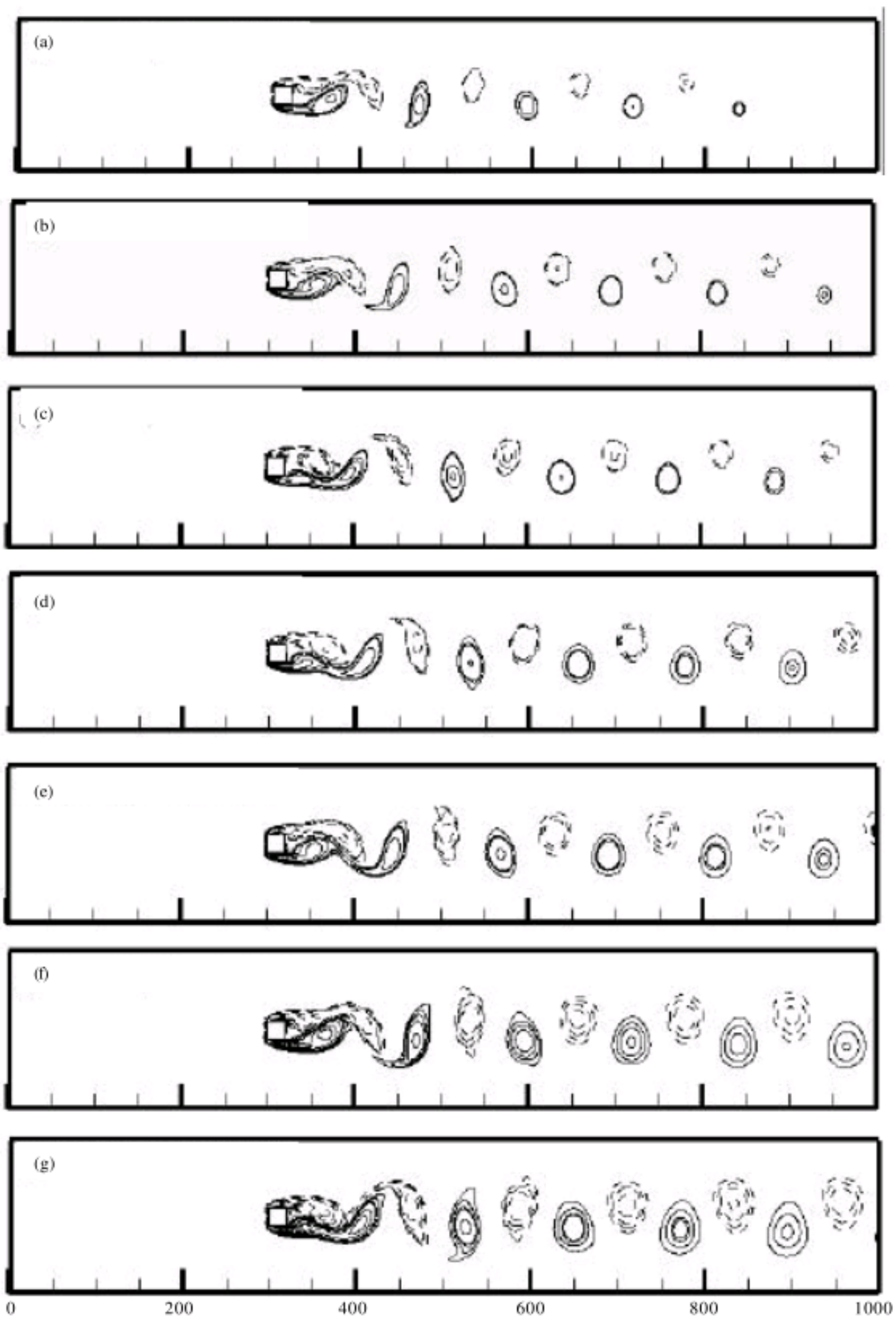

Fig. 5: Vorticity contour lines for simulation of flow past a square cylinder at $R_e = 100$ for different relaxation time parameter τ, (a) $R_e = 100$, Tau = 0.509, (b) $R_e = 100$, Tau = 0.512, (c) $R_e = 100$, Tau = 0.518, (d) $R_e = 100$, Tau = 0.526, (e) $R_e = 100$, Tau = 0.53, (f) $R_e = 100$, Tau = 0.539 and (g) $R_e = 100$, Tau = 0.548

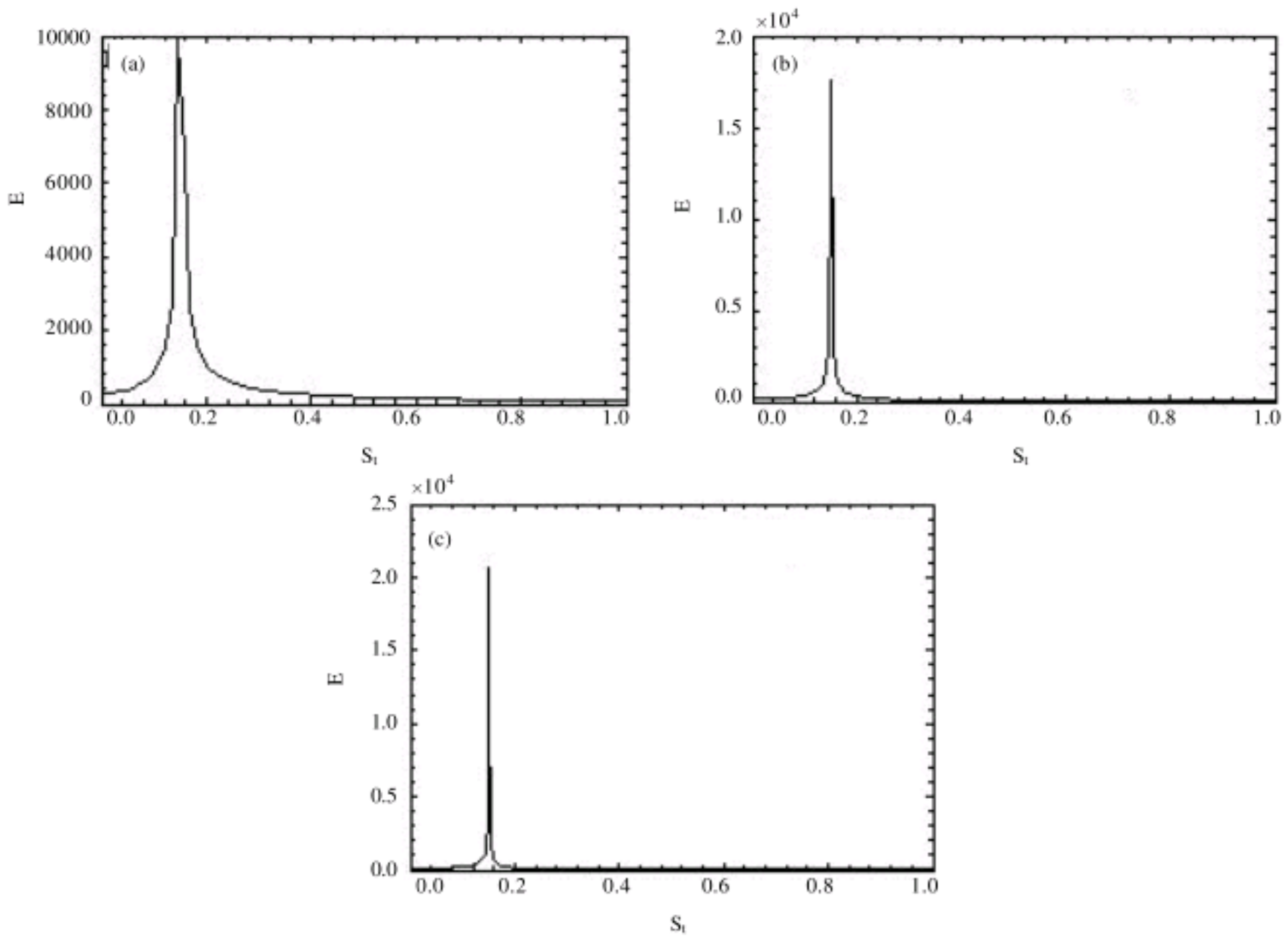

Fig. 6: The variation of power spectra or different relaxation time parameters, (a) $R_e = 100$, $\tau = 0.509$, (b) $R_e = 100$, $\tau = 0.526$ and (c) $R_e = 100$, $\tau = 0.548$

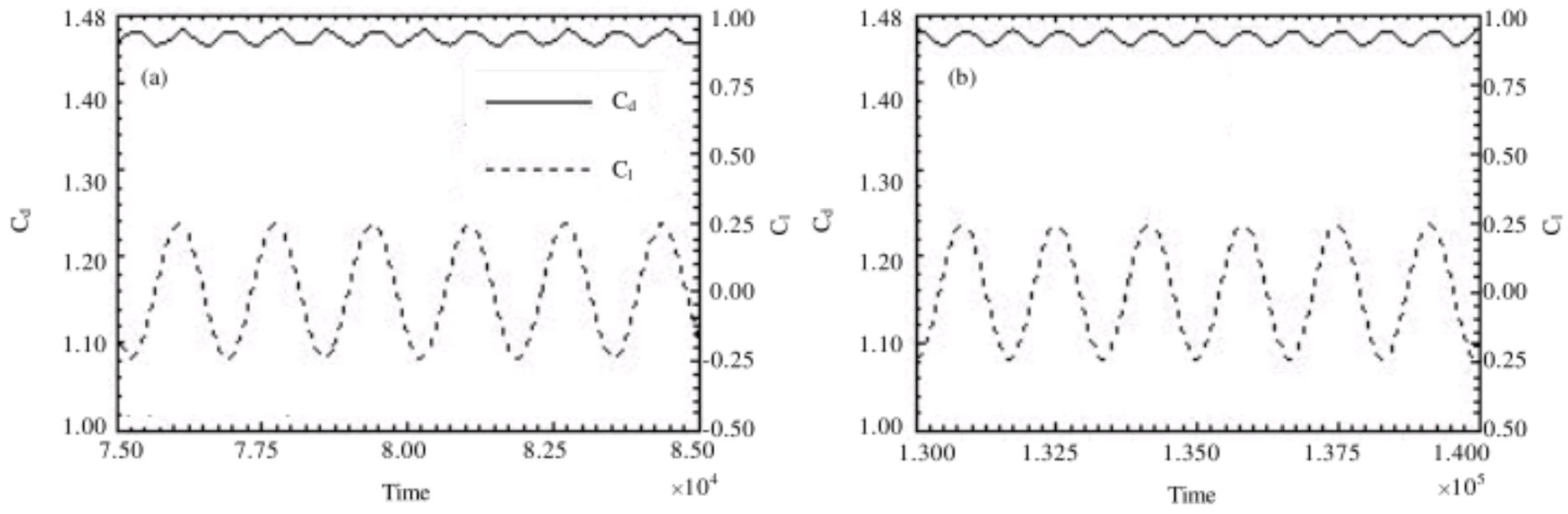

Fig. 7: Variation of drag and lift coefficients, (a) $R_e = 100$, $\tau = 0.548$ and (b) $R_e = 100$, $\tau = 0.548$

The formation of vorticity contour lines behind square cylinder for different inflow locations is clear from the Fig. 9a-e.

Figure 10 shows the comparison of the time evolution of C_l for three different cases $L_1 = 1.5$, 6 and 15 d.

Figure 11a-d show the Strouhal numbers for different inflow locations.

Figure 12 a and b show the drag and lift coefficients history developments for different inflow locations.

Available experimental and numerical data for different outflow locations have been compared to the corresponding computation results in Fig. 13a and b.

The formation of vorticity contour lines behind square cylinder for different downstream boundary locations is clear from Fig. 14a-f.

Figure 15 shows the variation of lift coefficient (C_l) with respect to time for three different outflow boundary locations $L_2 = 6$, 22 and 35 d.

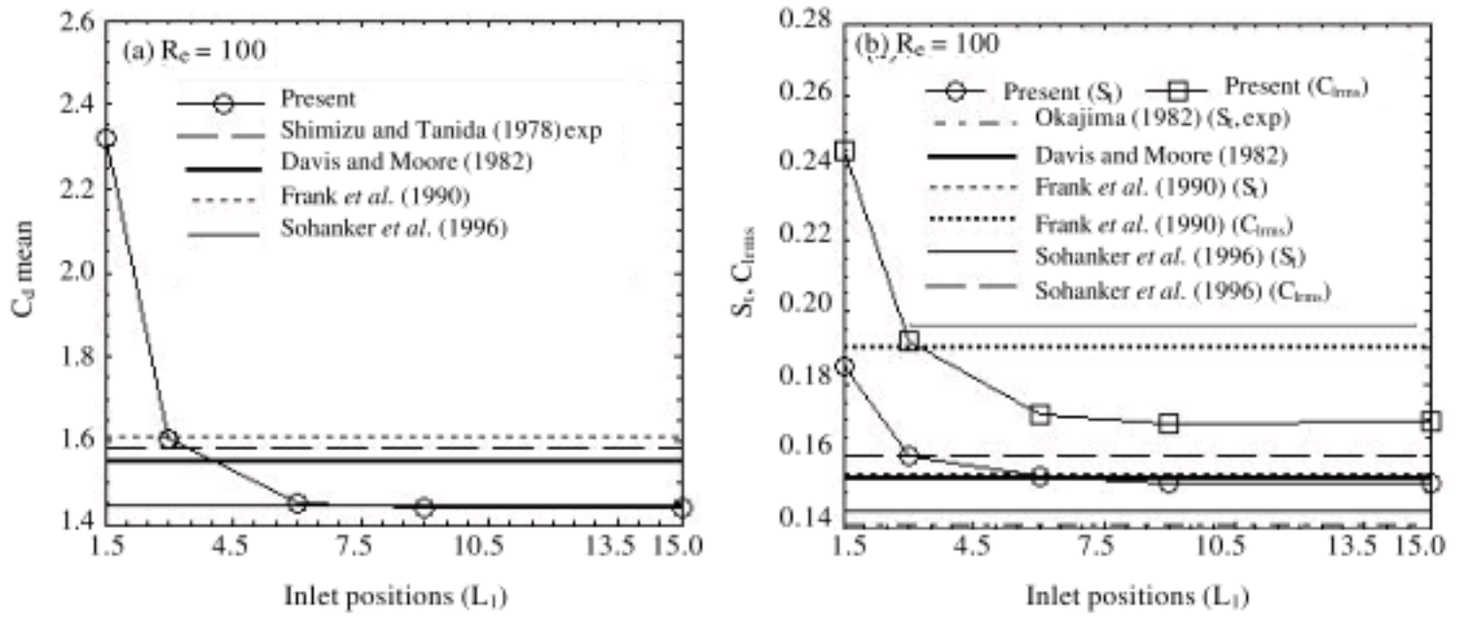

Fig. 8: (a) Comparison among a mean drag coefficient and (b) root mean square value of lift coefficient and Strouhal number results for the flow past a square cylinder for different upstream locations

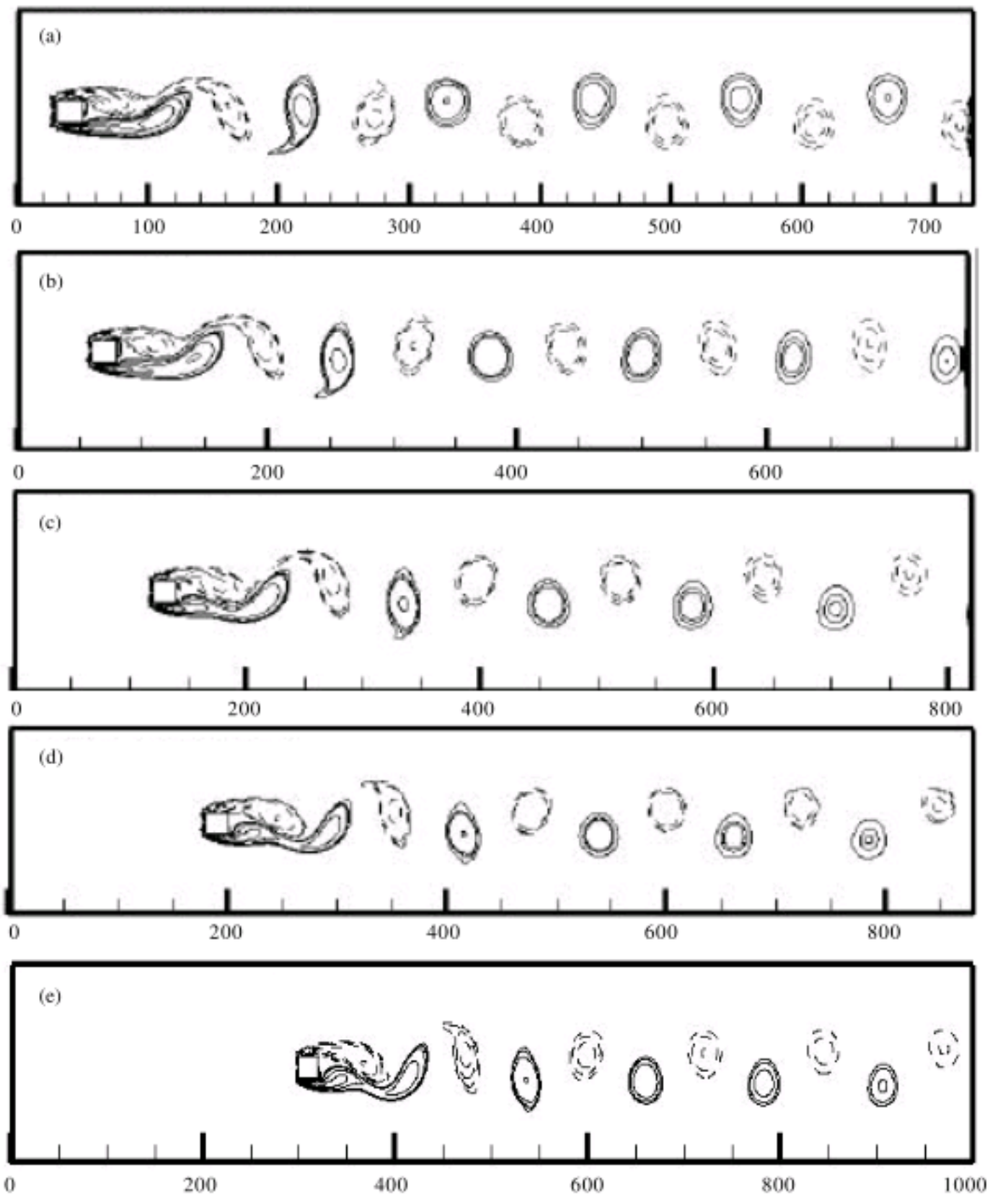

Fig. 9: Vorticity contour lines for simulation of flow past a square cylinder at R_e = 100 for different upstream locations, (a) R_e = 100, L_1 = 1.5 d, (b) R_e = 100, L_1 = 3 d, (c) R_e = 100, L_1 = 6 d, (d) R_e = 100, L_1 = 9 d and (e) R_e = 100, L_1 = 15 d

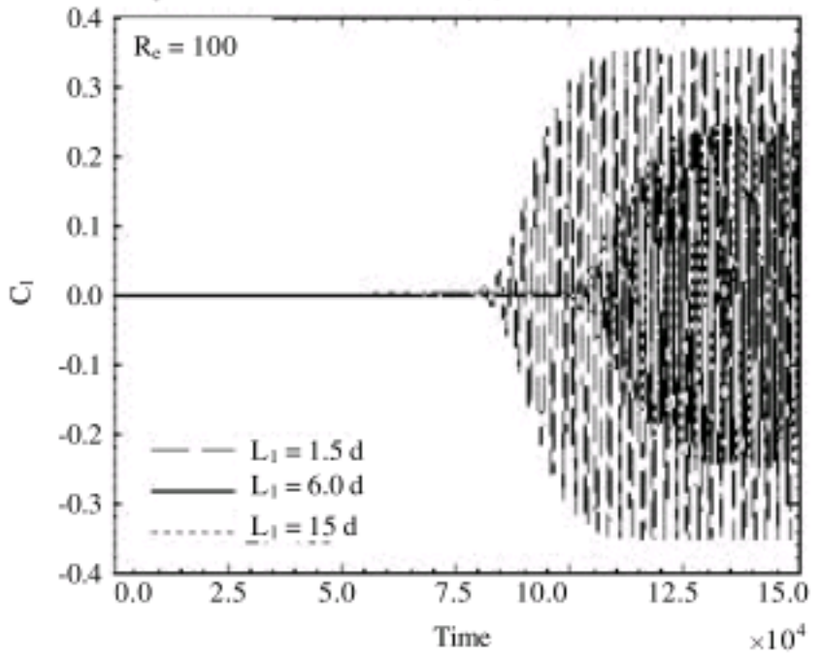

Fig. 10: Variation of lift coefficient with respect to time for different inlet positions

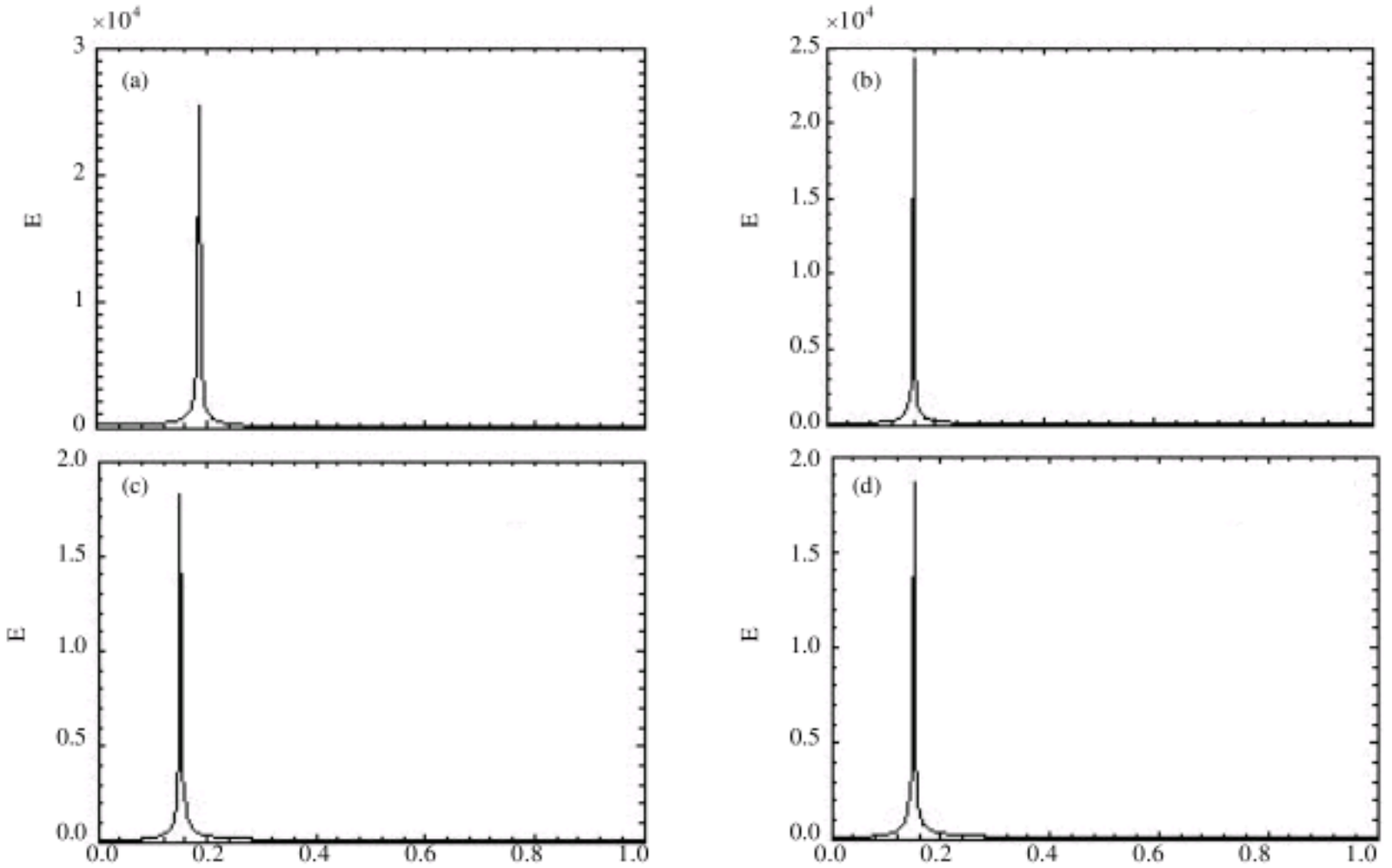

Fig. 11: The variation of power spectra for different inflow locations, (a) R_e = 100, L_1 = 1.5 d, (b) R_e = 100, L_1 = 3 d, (c) R_e = 100, L_1 = 6 d and (d) R_e = 100, L_1 = 15 d

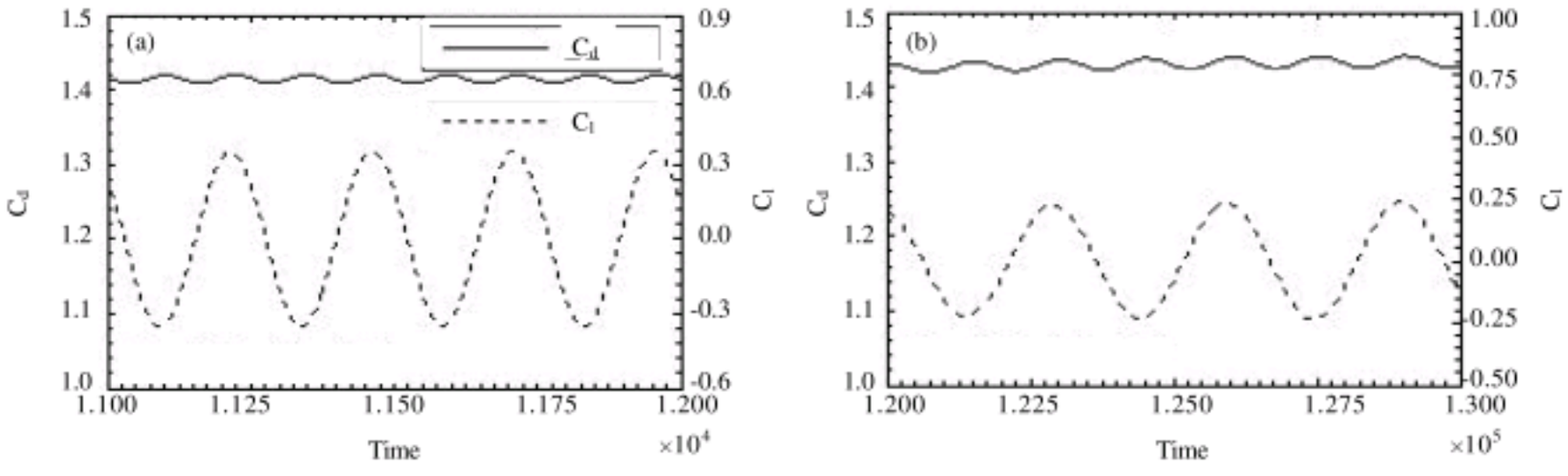

Fig. 12: Variations of drag and lift coefficients for different inflow positions, (a) R_e = 100, L_1 = 1.5 d and (b) R_e = 100, L_1 = 15 d

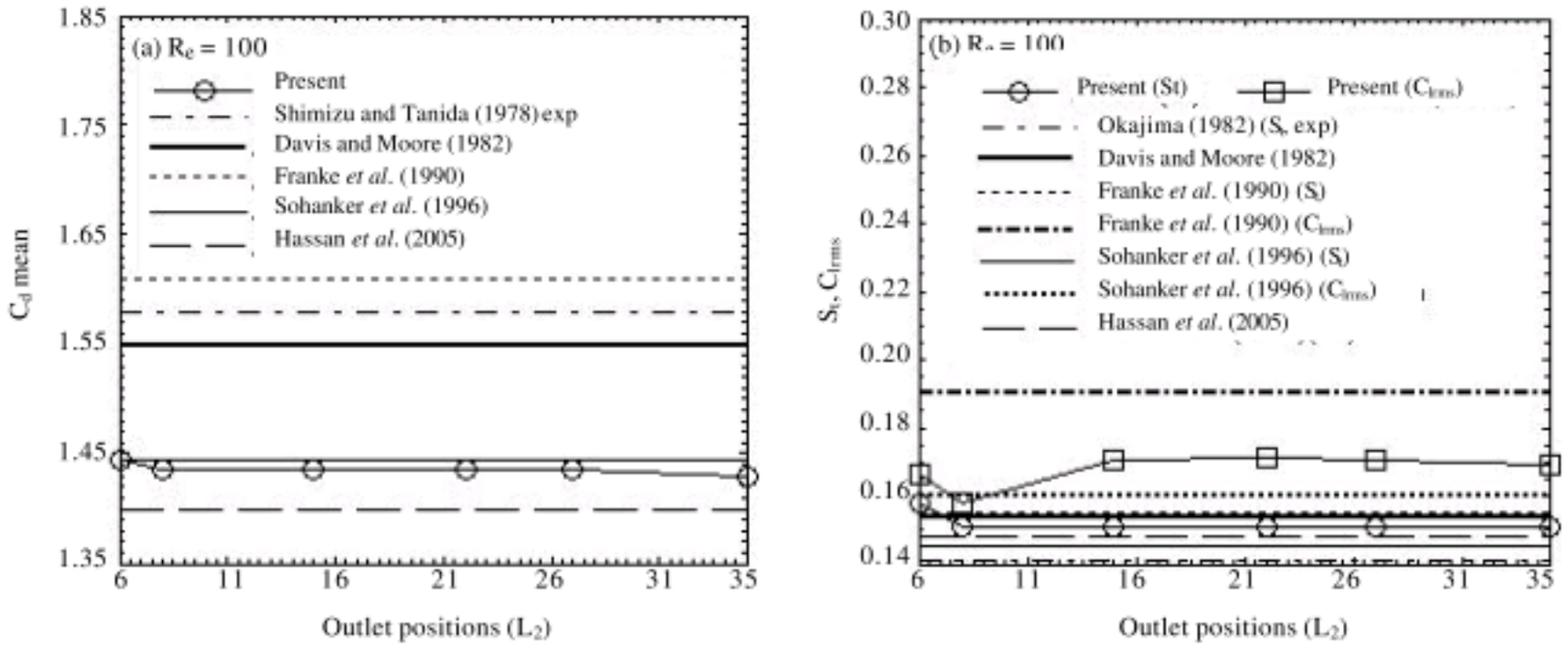

Fig. 13: (a) Comparison among a mean drag coefficient and (b) root mean square value of lift coefficient and Strouhal number results for the flow past a square cylinder for different upstream locations

We note here again that the Strouhal number is not sensitive to the downstream locations as can be seen in Fig. 16 a-d for different outflow locations.

Figure 17a-d show the drag and lift coefficients history developments for different outflow boundary locations.

A comparison between our results from periodic and symmetric boundary conditions for side wall locations and those from other researchers is made in Fig. 18a-c.

The formation of vorticity contour lines behind square cylinder for different wall boundary locations is clear from Fig. 19a-h for symmetric wall boundary condition and in Fig. 20a-h for periodic boundary condition.

Figure 21a-d and 22a-d show the power spectra for various side wall locations at R_e = 100 for periodic and symmetry boundary conditions, respectively.

The time histories of the lift and drag coefficients are plotted in Fig. 23a-d for periodic boundary condition and Fig. 24a-d for symmetric boundary condition.

To illustrate the effect of relaxation time parameter τ, we have performed a series of computations ranging from 0.509 to 0.548 for low Mach numbers. We choose $\tau = 0.526$ for comparison here to examine the differences between the present and previous available results from open literature data. The selection of $\tau = 0.526$ have some reasons. When the values of τ decreases from 0.526 to 0.509, the approximate deviation between physical quantities such as mean drag coefficient is almost negligible. While on the other hand in case of 0.509 need three times more computational time as compared to 0.526 (Fig. 3). Whenever, the value of τ increases from 0.526 to 0.548, the physical quantities such as mean drag coefficient increases up to some extent (Fig. 4a, b). In order to asses the influence of relaxation time parameter τ, we have computed mean drag coefficients, root mean square value of lift coefficient and Strouhal number for flow past a square cylinder and compared with the results due to Davis and Moore (1982), Franke *et al*. (1990), Sohankar *et al*. (1996), Okajima (1982) and Shimizu and Tanida (1978). Present results are slightly better than with those of Franke *et al*. (1990), Davis and Moore (1982) and Shimizu and Tanida (1978). The maximum percentage difference of mean drag coefficient and Strouhal number from the results due to Davis and Moore (1982) is about 12.1, 12.52 and 1.4%, respectively. The maximum difference of our mean drag coefficient with Shimizu and Tanida (1978) at R_e = 100 is 9.21%. The deviation for Strouhal number with Franke *et al*. (1990) and Sohankar *et al*. (1996) is approximately 2 and 5.5%, respectively. It may be noted that present computed results agrees well with Sohankar *et al*. (1996) for mean drag coefficient and Strouhal number for $\tau = 0.526$.

Vortex shedding is a comprehensive physical phenomenon. When it occurs, vortices are shed alternatively from the top and bottom of the cylinder. Figure 5a-g shows the patterns of vorticity contour lines. In Fig. 5a-g the dashed lines represents the negative vorticity (clockwise vortex) and the solid lines represents the positive vorticity (anticlockwise vortex). The negative vortex is rolling up on the upper side of the cylinder while the positive vortex appears on the lower side of the cylinder (Fig. 5a, b). While the positive vortex is reforming and the negative vortex is being shed at τ = 0.518 and 0.526 (Fig. 5c, d). Figure 5e shows that at τ = 0.530, a positive vortex is in the process of development on lower side of the cylinder, while a negative vortex is about to detach from the cylinder. While at $\tau = 0.539$ (Fig. 5f), from

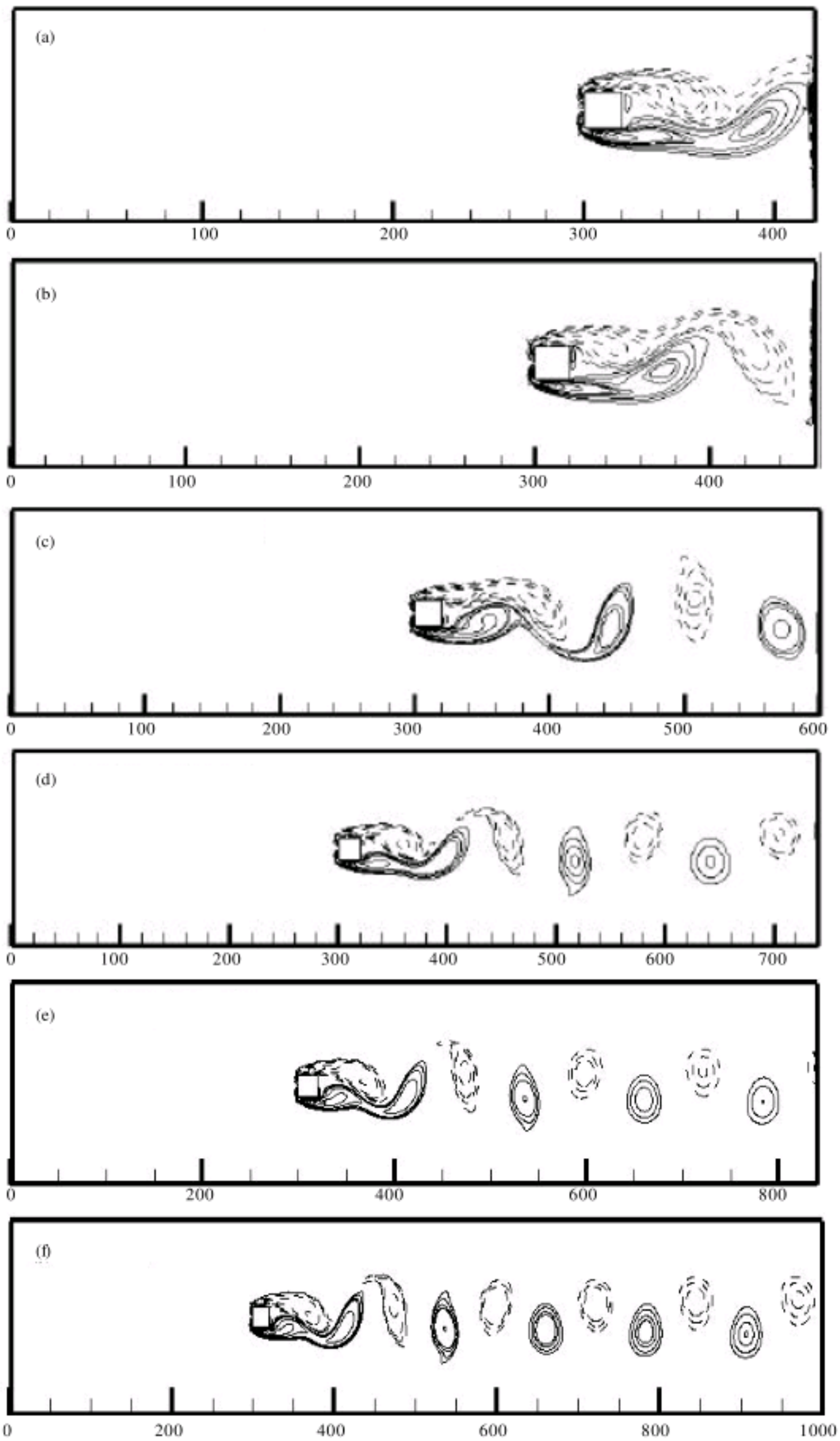

Fig. 14: Vorticity contour lines for simulation of flow past a square cylinder at R_e = 100 for different outflow locations, (a) R_e = 100, L_2 = 6 d, (b) R_e = 100, L_2 = 8 d, (c) R_e = 100, L_2 = 15 d, (d) R_e = 100, L_2 = 22 d, (e) R_e = 100, L_2 = 27 d and (f) R_e = 100, L_2 = 35 d

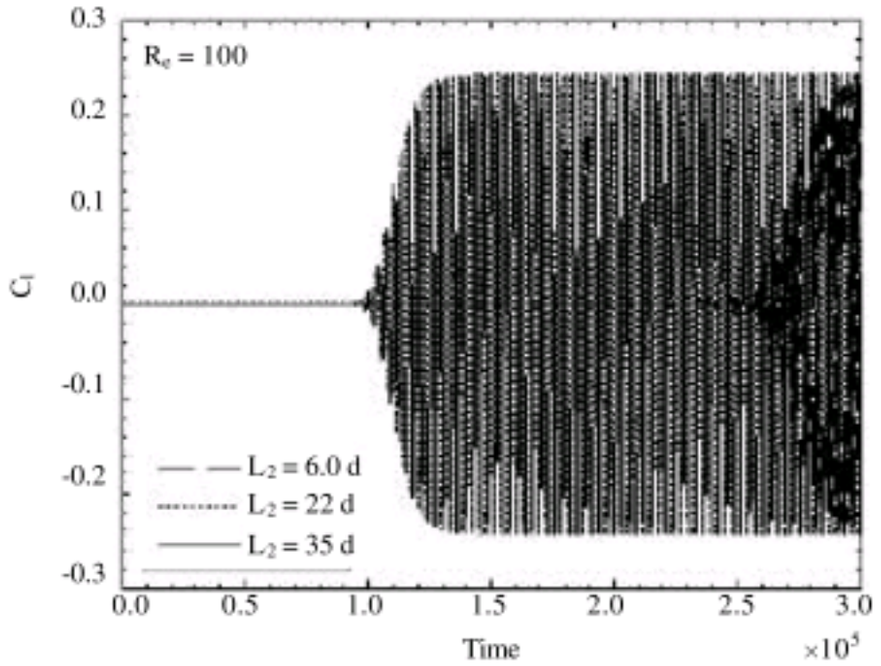

Fig. 15: The time history of lift coefficient for three different outflow boundary locations

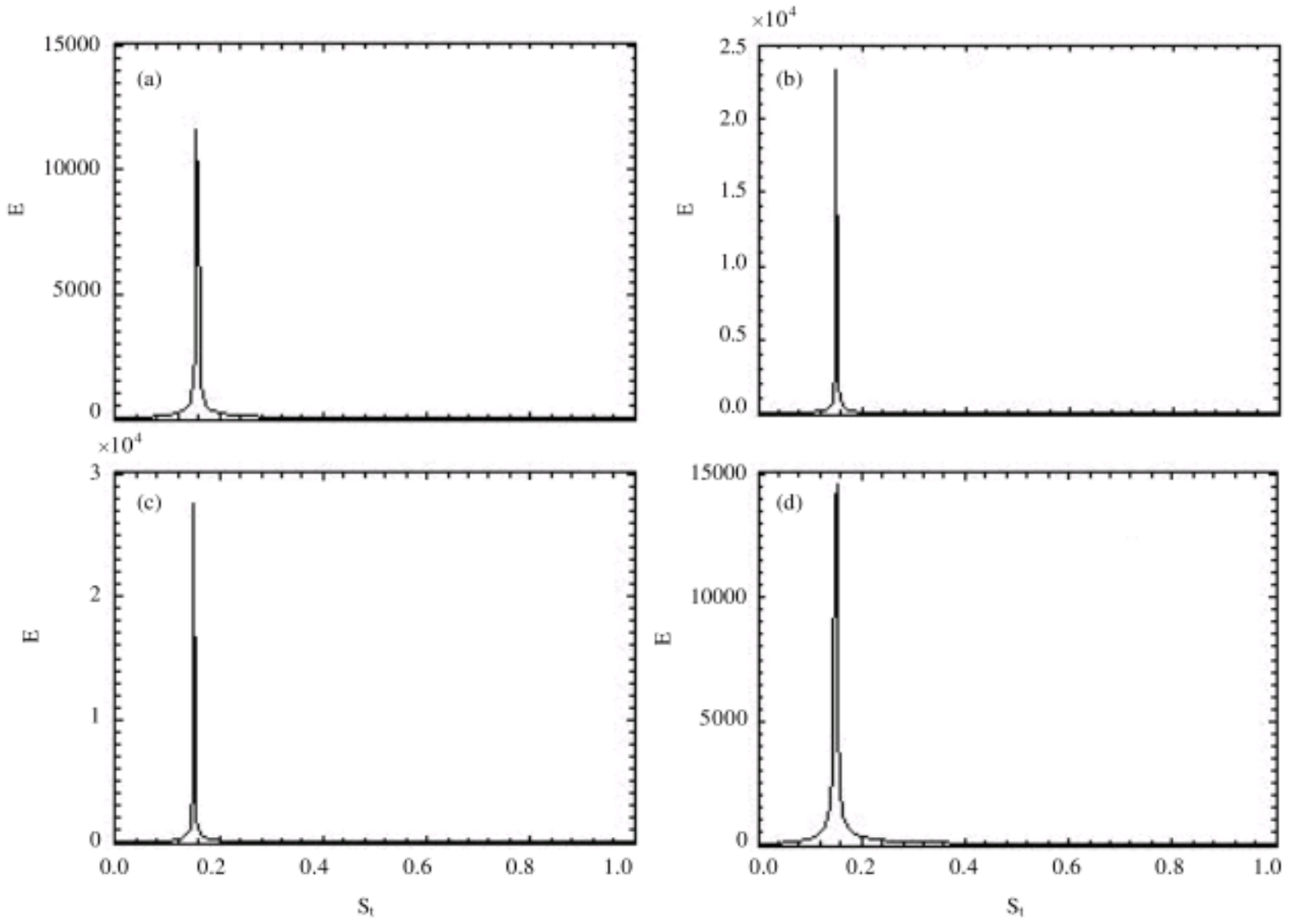

Fig. 16: The variation of power spectra for different outflow boundary locations using FFT, (a) R_e = 100, L_2 = 6 d, (b) R_e = 100, L_2 = 8 d, (c) R_e = 100, L_2 = 22 d and (d) R_e = 100, L_2 = 35 d

the upper side of the wake the positive vortex draws the shear layer of opposite sign and cuts the supply of vorticity to the positive vortex at the wake centerline τ = 0.548, Fig. 5g). It is observed that the two main vortexes after the cylinder interact with each other to generate positive and negative vortices alternately. When τ are slightly increase from 0.56 to 0.548, each individual vortex is stronger and more round. While on other hand, the vortices almost disappear in the far wake. The differences in the size and strength of the alternately shed vortices become more pronounced with different τ. We note here that the Strouhal numbers is not so much affected for chosen relaxation time parameter values (Fig. 6a-c).

The results show that the drag coefficient shown in Fig. 7a, is not a simple sine wave and there seems to be a

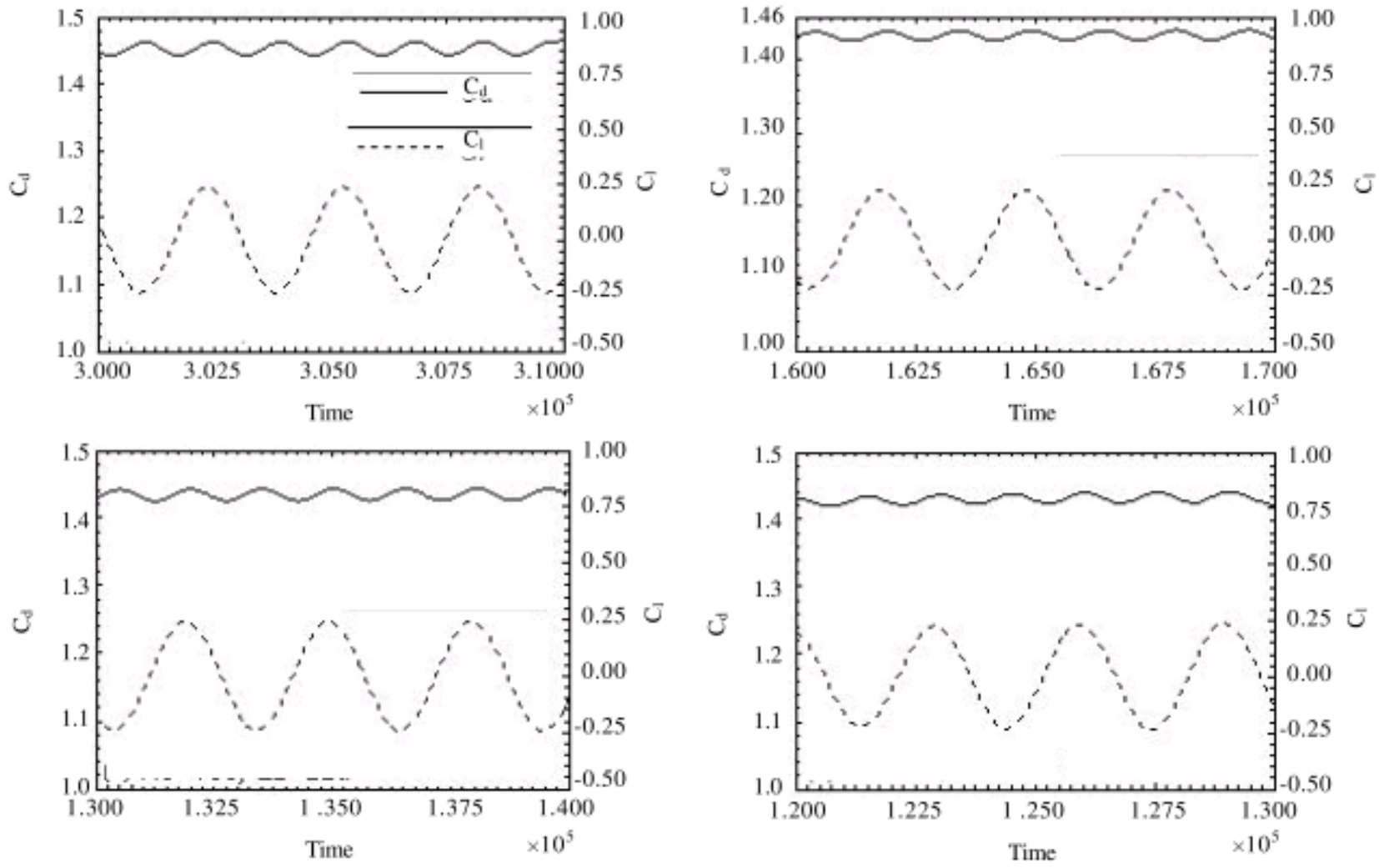

Fig. 17: Variations of drag and lift coefficients for different outflow boundary conditions, (a) $R_e = 100$, $L_2 = 6$ d, (b) $R_e = 100$, $L_2 = 8$ d, (c) $R_e = 100$, $L_2 = 22$ d and (d) $R_e = 100$, $L_2 = 35$ d

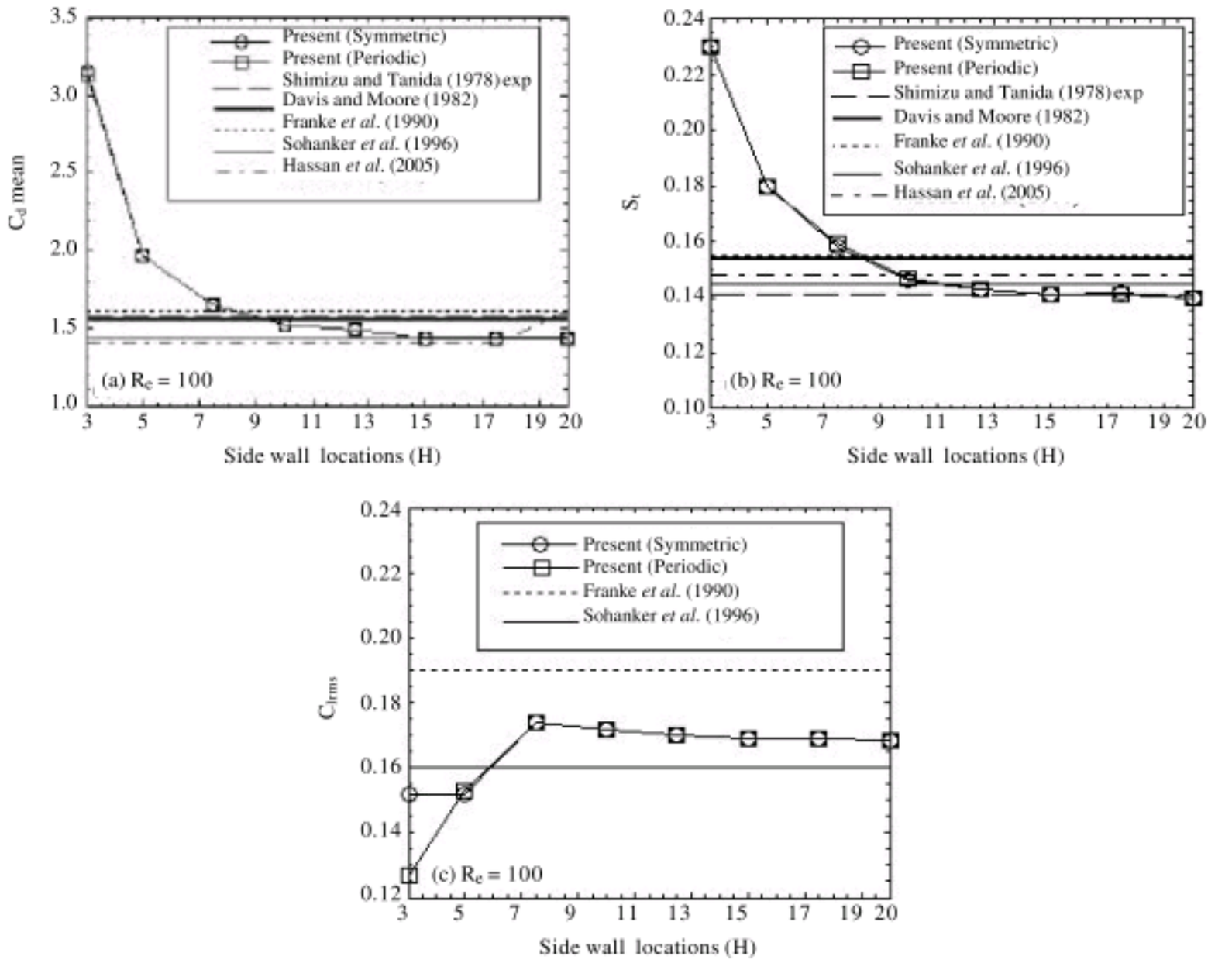

Fig. 18: (a) Comparison among a mean drag coefficient (b) Strouhal number and (c) root mean square value of lift coefficient results for the flow past a square cylinder for different upstream locations

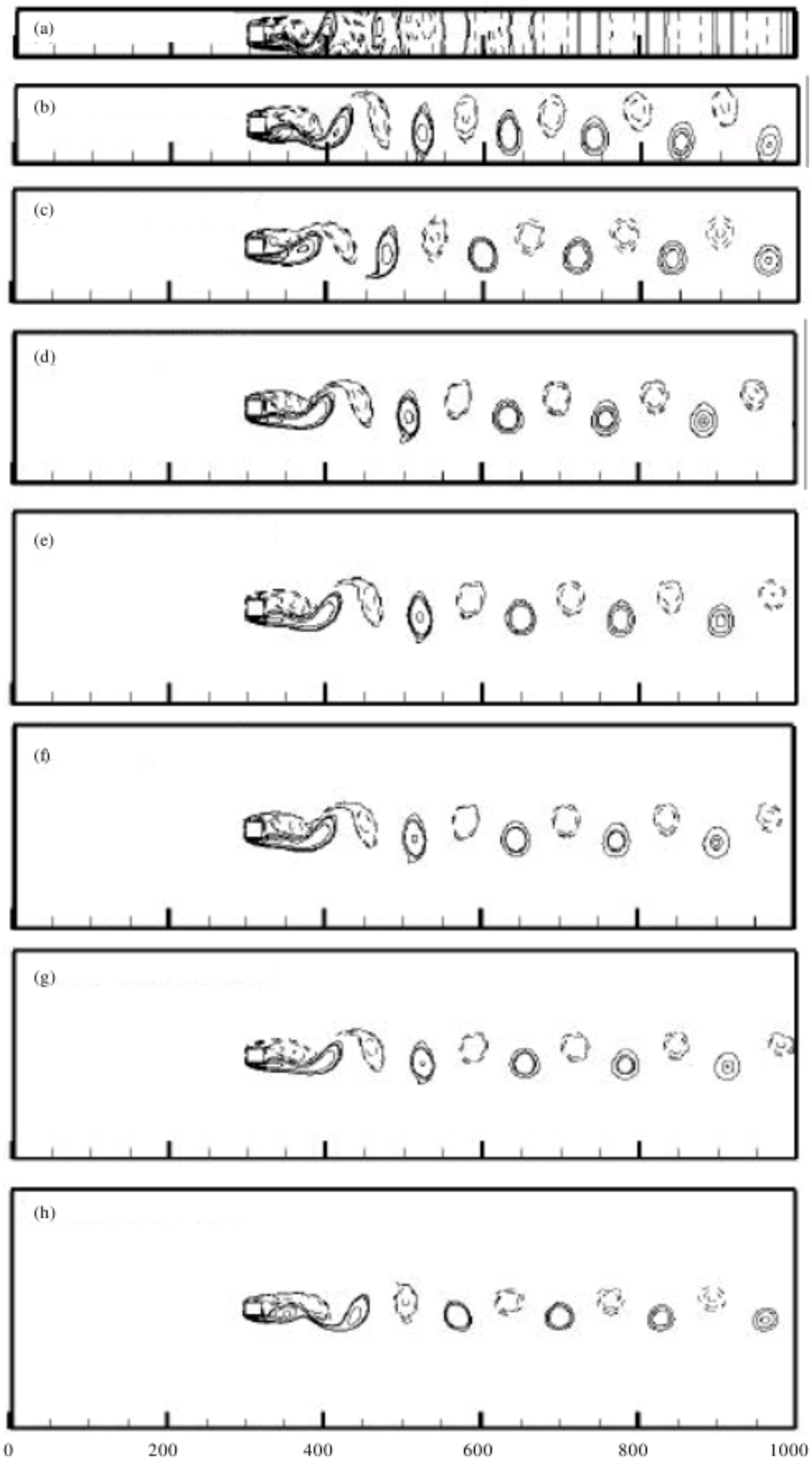

Fig. 19: Vorticity contour lines for simulation of flow past a square cylinder at R_e = 100 for different side wall locations using symmetric boundary condition, (a) R_e = 100, H = 3 d, (b) R_e = 100, H = 5 d, (c) R_e = 100, H = 7.5 d, (d) R_e = 100, H = 10 d, (e) R_e = 100, H = 12.5 d, (f) R_e = 100, H = 15 d, (g) R_e = 100, H = 17.5 d and (h) R_e = 100, H = 20 d

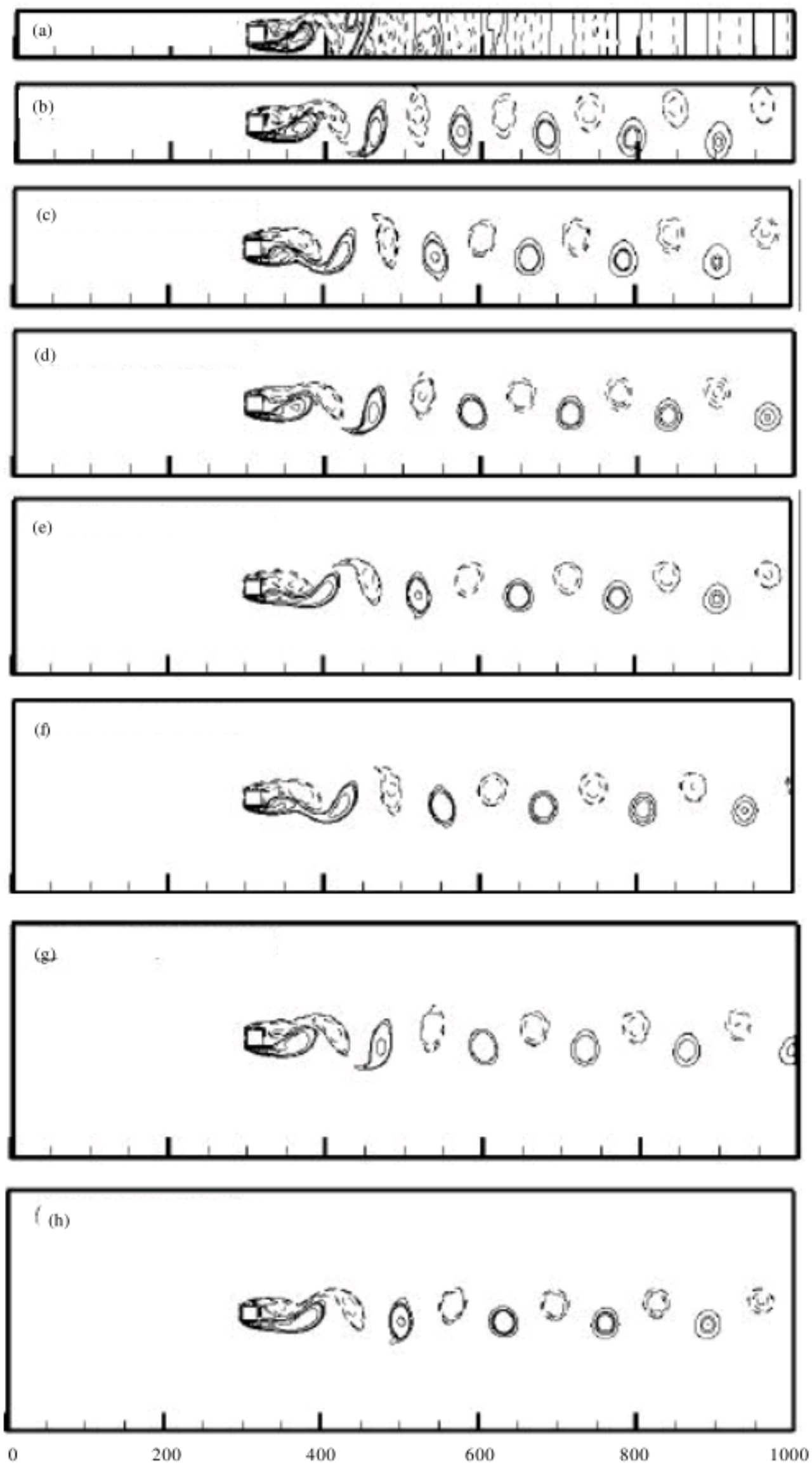

Fig. 20: Vorticity contour lines for simulation of flow past a square cylinder at $R_e = 100$ for different side wall locations suing the periodic boundary conditions, (a) $R_e = 100$, H = 3 d, (b) $R_e = 100$, H = 5 d, (c) $R_e = 100$, H = 7.5 d, (d) $R_e = 100$, H = 10 d, (e) $R_e = 100$, H = 12.5 d, (f) $R_e = 100$, H = 15 d, (g) $R_e = 100$, H = 17.5 d and (h) $R_e = 100$, H = 20 d

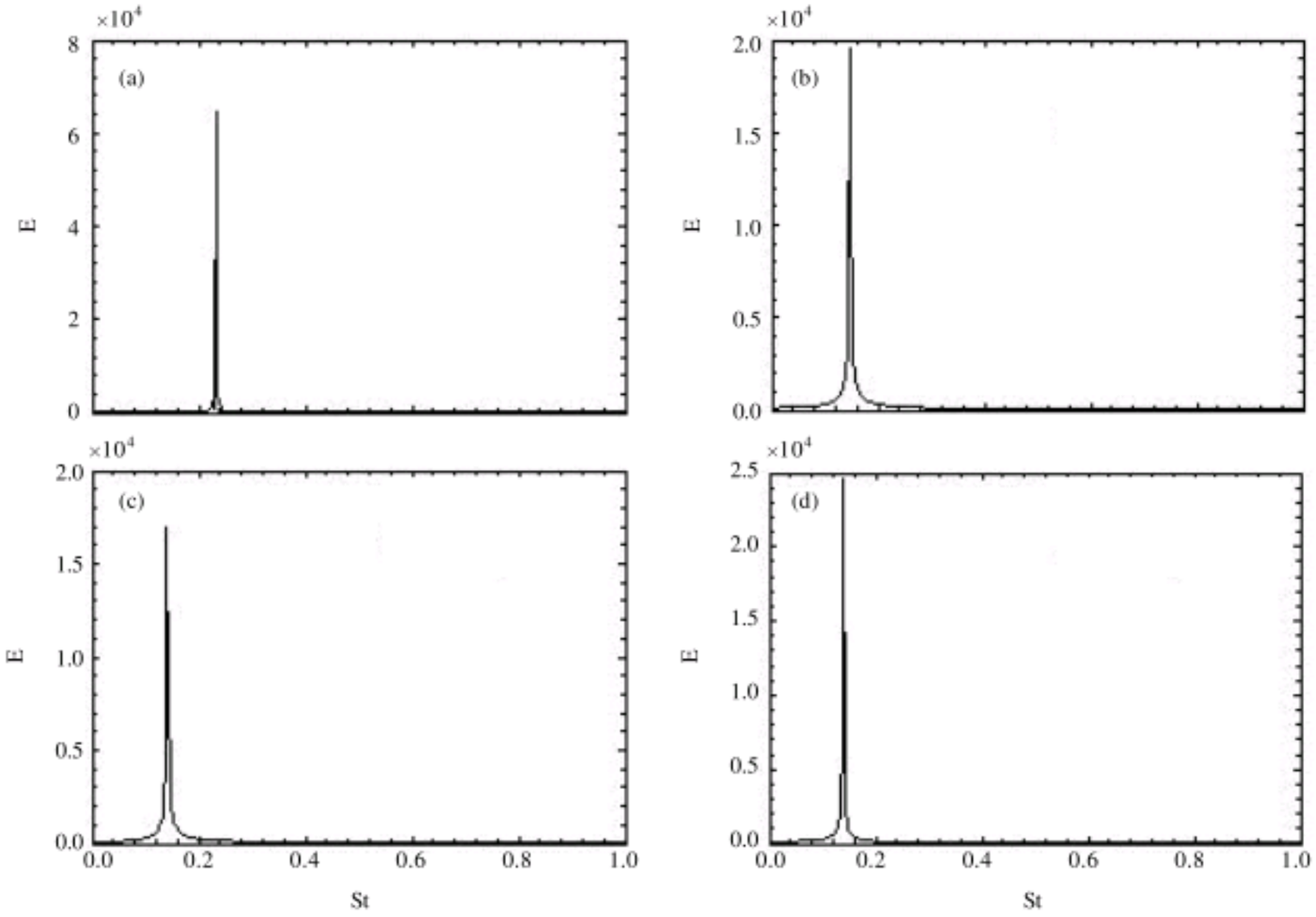

Fig. 21: The variation of power spectra for different side wall locations using FFT, (a) Periodic R_e = 100, H = 3 d, (b) Periodic R_e = 100, H = 10 d, (c) Periodic R_e = 100, H = 15 d and (d) Periodic R_e = 100, H = 20 d

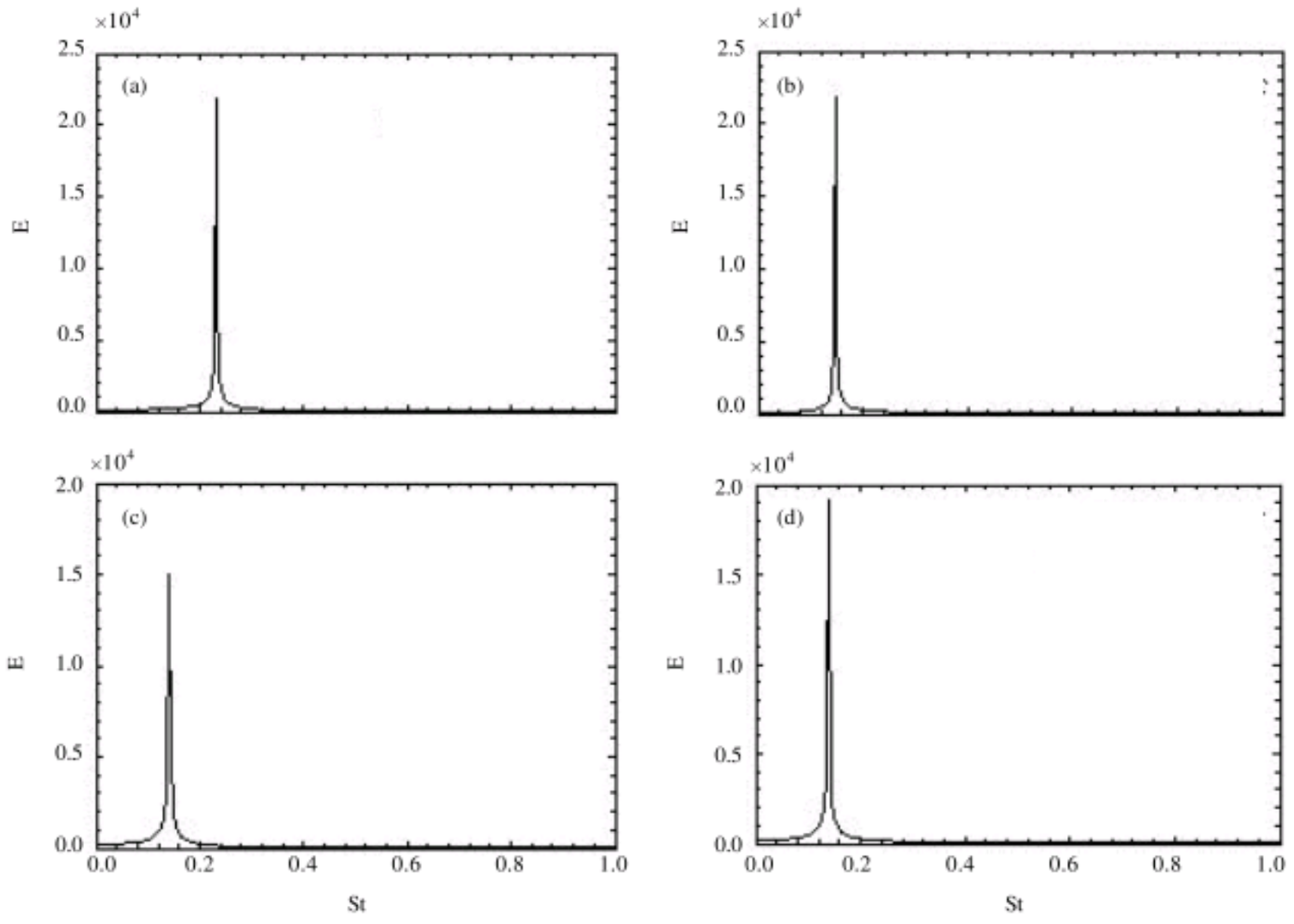

Fig. 22: The variation of power spectra for different side wall locations using FFT, (a) Symmetric R_e = 100, H = 3 d, (b) Symmetric R_e = 100, H = 10 d, (c)Symmetric R_e = 100, H = 15 d and (d) Symmetric R_e = 100, H = 20 d

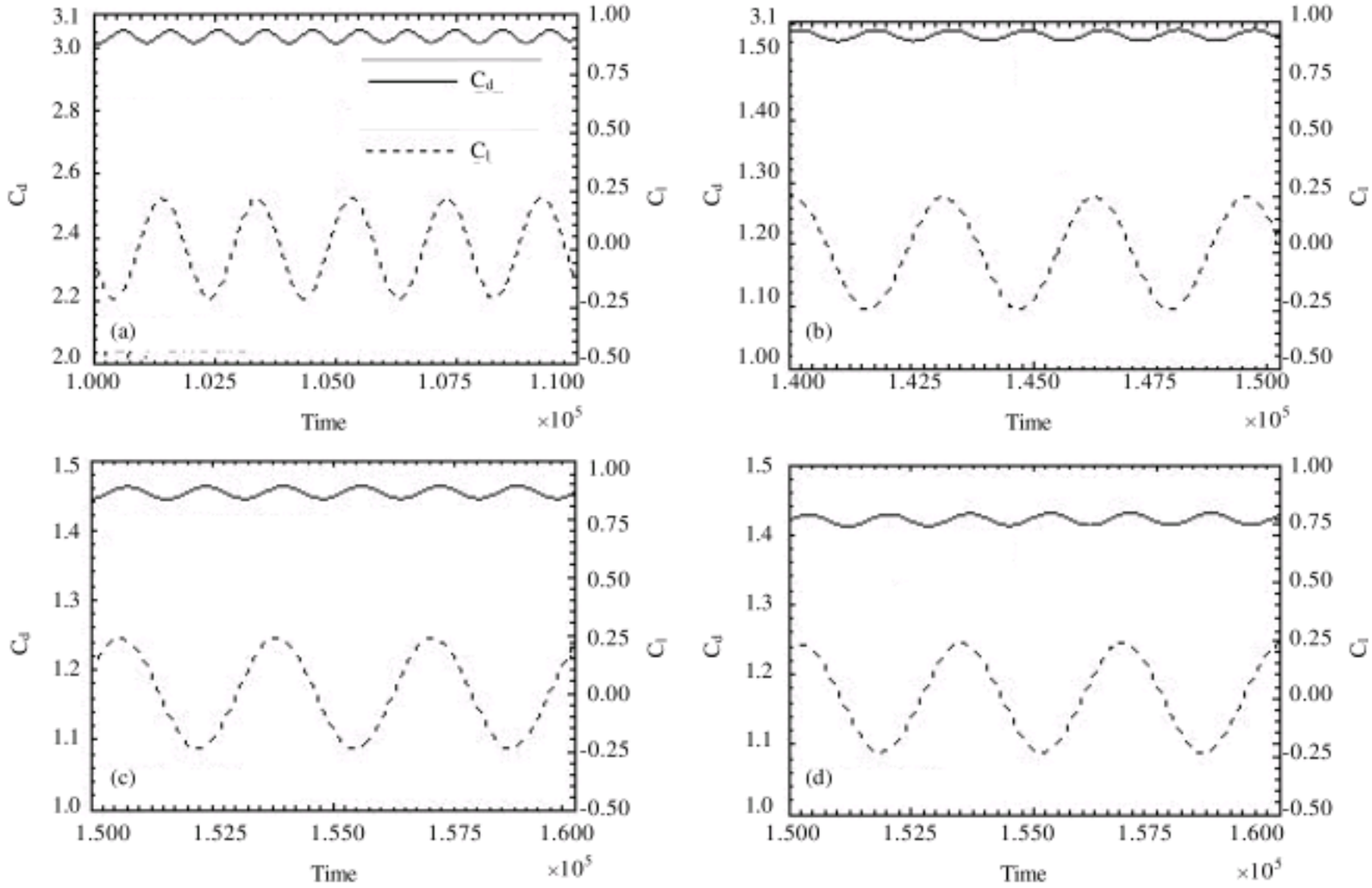

Fig. 23: Variations of drag and lift coefficients for different side wall locations, (a) Periodic R_e = 100, H = 3 d, (b) Periodic R_e = 100, H = 10 d, (c) Periodic R_e = 100, H = 15 d and (d) Periodic R_e = 100, H = 20 d

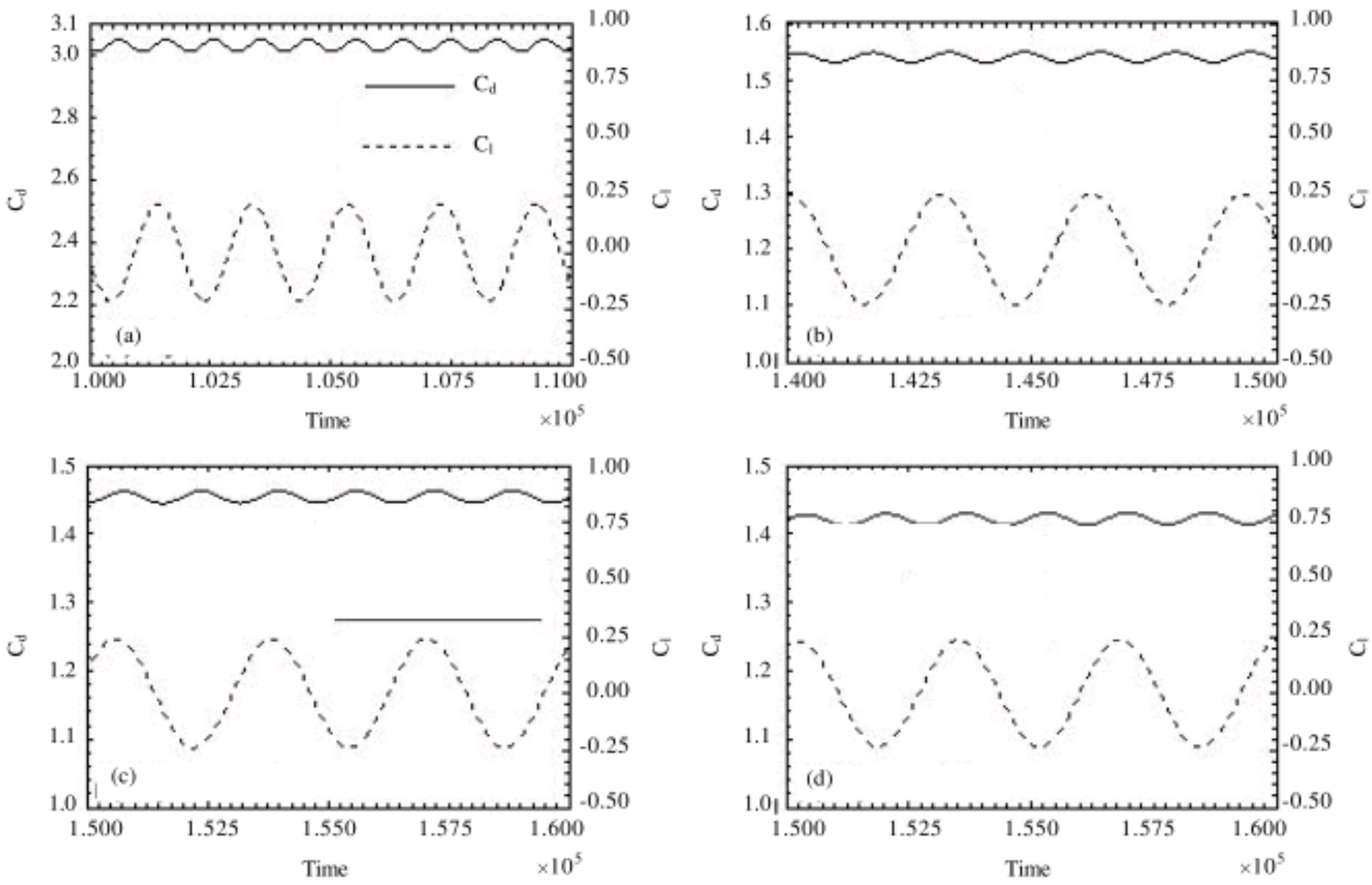

Fig. 24: Variations of drag and lift coefficients for different side wall locations, (a) Symmetric R_e = 100, H = 3 d, (b) Symmetric R_e = 100, H = 10 d, (c) Symmetric R_e = 100, H = 15 d and (d) Symmetric R_e = 100, H = 20 d

small modulation in shedding frequency. While on the other hand for running more time the results show that the vortex shedding becomes periodic and the frequency of the lift coefficient is twice that of the drag coefficient (Fig. 7b). This observation shows that the selection of $\tau = 0.526$ is a reasonable choice for flow past a square cylinder at $R_e = 100$. As expected the relaxation time parameter affects the flow characterize parameters and the development process of vortex shedding. The above observations indicate that the simulation time, physical quantities such as mean drag coefficients and vortex shedding depends on the value of relaxation time parameter τ.

In order to assess the influence of upstream locations, we have computed the mean drag coefficients, root mean square value of lift coefficient and Strouhal number for flow past a square cylinder for fixed value of R_e and compared with the results due to Davis and Moore (1982), Franke *et al*. (1990), Sohankar *et al*. (1996), Okajima (1982) and Shimizu and Tanida (1978) (Fig. 8a, b). Present results for $L_1 = 15$ d are in excellent agreement with Sohankar *et al*. (1996) and slightly better than other results. The maximum deviation of Strouhal number from the results due to Davis and Moore (1982), Franke *et al*. (1990), Sohankar *et al*. (1996) and Okajima (1982) are 1.17, 2.01, 5 and 7%, respectively. Present computed results for mean drag coefficient differ from Davis and Moore (1982) results by 7% and from Shimizu and Tanida (1978) by 8.7%. Comparable present results for root mean square value of lift coefficient with Franke *et al*. (1990) and Sohankar *et al*. (1996), indicating a maximum difference about 10.4 and 1.8%, respectively. It can be seen from Fig. 8a and b that the approximate deviations between mean drag coefficient, root mean square value of lift coefficient and Strouhal number, is about 48.8, 44 and 21.5%, respectively, when the cylinder brought near to the inlet boundary from 15 to 1.5 d for present numerical data.

The shedding of vortices is always accompanied by some physical changes in the local flow. The negative vortex is generated at the top corner of the cylinder and more behind the cylinder as it grows and is rolling up on the upper side of the cylinder (Fig. 9a, b). The long negative vortex has cut off the supply between the lower shear layer and the positive vortex (Fig. 9c). The negative vortex is being generated and the positive one on the other side is reforming (Fig. 9d, e). Formations of the positive and negative vortexes are completed, when the vortexes are transported downstream by the flow field. It is observed that the vortices are shed alternately, with positive and negative vortices. The differences in the size and strength of the alternately shed vortices are more pronounced as the upstream locations change from 1.5 to 15 d. It seems that the growth rate and the frequency of the perturbations are not affected so much. The results further show that the inlet positions affected the computational time upto some extend. Another interesting feature that there is no distortion when the inlet position varied from $L_1 = 1.5$ to 15 d (Fig. 10). We observed that the Strouhal number is not sensitive to the upstream locations as can be seen in Fig. 11a-d. Figure 12a and b show the drag and lift coefficients history developments. The results show that the vortex shedding becomes periodic and the frequency of the lift coefficient is twice that of the drag coefficient, which are consistent with those of Davis *et al*. (1984). A comparison of the performance of the various inlet positions will allow us to choose the best inlet position for our simulations. We take $L_1 = 15$ din all numerical calculations.

Available experimental data for mean drag coefficient and Strouhal number of Davis and Moore (1982), numerical data for mean drag coefficient and Strouhal number of Franke *et al*. (1990), numerical data for mean drag coefficient, root mean square value of lift coefficient and Strouhal number of Sohankar *et al*. (1996), experimental data for Strouhal number of Okajima (1982), experimental data for mean drag coefficient of Shimizu and Tanida (1978) and numerical data for mean drag coefficient and Strouhal number of Hassan *et al*. (2005) have been compared to the corresponding computation results in Fig. 13a, b for different outflow locations. It can be seen that parameters like root mean square value of lift coefficient and Strouhal number for outlet boundary $L_2 = 35$ d, differ about 1 and 5.1% from the value reported by Sohankar *et al*. (1996). The results further show that the mean drag coefficient is decrease about 9.4% from the experimental value reported by Shimizu and Tanida (1978) and show a good agreement with the numerical data of Hassan *et al*. (2005) with 2.42%. However, the deviation in Strouhal number is about 6.8% from the experimental value reported by Okajima (1982) and numerical results reported by Davis and Moore (1982) about 1.4%, Hassan *et al*. (2005) about 1.9% and Franke *et al*. (1990) about 2.01%, respectively. We also observed that for $L_2 = 35$ dthe root mean square value of lift coefficient slightly decreases and then slightly increased for further outlet boundary locations and finally with a slight decreased for further downstream boundary locations. However, it is also found that there is a slight difference for physical quantities and the vortex formation for two outlet boundary locations $L_2 = 27$ and 35 d. The increase in mean drag coefficient, root mean square value of lift coefficient and Strouhal number as the outlet boundary brought closer from 35 to 6 d is about 1.3, 1.62 and 4.4%, respectively.

The formation of vorticity contour lines behind square cylinder for different outflow locations is clear from Fig. 14a-f. A positive vortex appears on the lower side of the cylinder and a negative vortex is rolling up on the upper side of the cylinder, but eventually the outlet boundary cuts the development process of negative vortex (Fig. 14a). The similar process happened again and the negative vortex developed fully but further alternating shed is stopped because of closed outlet boundary locations (Fig. 14b). While the negative vortex is being shed and the positive one on the other side is reforming because of little wider outlet boundary location as compared to the first two observations (Fig. 14c). Figure 14d shows that a positive vortex is in the process of development on lower side of the cylinder, while a negative vortex is about to detach from the cylinder and from the upper side also the negative vortex is in completion process. The same phenomena occur again but this time the negative vortex is completed (Fig. 14e). The vortex is transported downstream by the flow field and formation of the positive vortex is completed (Fig. 14f). It is interesting observation that when the outlet boundary locations are much closed to the body, the flow field stress to developed the shedding and that's why we observed the considerable difference between the wake size at different boundary locations (Fig. 14 a-f). It can be seen that the frequency rate not affected so much for different outlet boundary locations. The results further show that the developing process of alternating shedding take more computational time for L_2 = 6 d as compared to L_2 = 35 d (Fig. 15). We note here again that the Strouhal number is not sensitive to the outflow locations as can be seen in Fig. 16a-d. The results show that the vortex shedding becomes periodic and the frequency of the lift coefficient is twice that of the drag coefficient, which are consistent with those of Davis *et al*. (1984) (Fig. 17a-d). A comparison of the performance of the various outlet positions will allow us to choose the best outlet position for present simulations. We take L_2 = 35 din all numerical calculations.

A comparison between our results from periodic and symmetric boundary conditions and those from other researchers Davis and Moore (1982), Franke *et al*. (1990), Sohankar *et al*. (1996), Okajima (1982), Shimizu and Tanida (1978) and Hassan *et al*. (2005) is made in Fig. 18a and b, in which the drag and mean drag coefficients, root mean square value of lift coefficient and Strouhal number at R_e = 100 are listed. The differences between periodic and symmetric boundary conditions for physical quantities are almost negligible (Fig. 18a-c). The periodic boundary condition shows slightly better results than symmetric boundary condition for some cases and the shedding start little earlier. For comparison with open literature data we choose the periodic boundary condition for different side wall locations. The maximum difference of our mean drag coefficient with Davis and Moore (1982) is about 9.3%, Shimizu and Tanida (1978) is about 9.6% and Hassan *et al*. (2005) is about 1.6%. The deviation between our results for Strouhal number and those of Davis and Moore (1982), Franke *et al*. (1990), Sohankar *et al*. (1996), Okajima (1982) and Hassan *et al*. (2005) is about 8.9, 9.5, 3.2, 1.6 and 3.1%, respectively. The deviation between the present results and numerical results from Franke *et al*. (1990) and Sohankar *et al*. (1996) is about 12.6 and 4.4%, respectively for root mean square value of lift coefficient. However, it can be seen that the root mean square value of lift coefficient and Strouhal number increases with an decrease in side wall locations from H = 20 to 3 d is about 9.6 and 24.8%, respectively. This behavior is in agreement with the numerical results of Fornberg (1991) and Ingham (1990) for flow past a row of circular cylinders and normal flat plates, respectively. The computed results also show that the root mean square value of lift coefficient show a slight increase or decrease for different wall boundary locations.

The formation of vorticity contour lines behind square cylinder for different wall boundary locations is clear from Fig. 19a-h for symmetric wall boundary condition and in Fig. 20a-h for periodic boundary condition. The very dense arrangements of vortices represent the higher value of the vortex-shedding Strouhal number (Fig. 19a, 20a). In such case, it show that there is not enough space in the lateral direction for the vortices to shed downstream further, as a result the vortices are cracked down by the closed location of side walls and seem to disappear in the far wake. Mostly, such phenomena occur during blockage investigation of confined walls. A negative vortex is about to detach from the cylinder, while the positive vortex is in the process of development on lower side of the cylinder (Fig. 19b, e, f). A negative vortex is rolling up on the upper side of the cylinder while a positive vortex appears on the lower side of the cylinder (Fig. 19c). Near to the wake centerline the supply of vorticity to the positive vortex cuts eventually, because the shear layer developed from the positive vortex show opposite sign from the upper side of the wake across (Fig. 19d). Formation of the positive vortex is almost completed (Fig. 19g, h), after which the vortex is transported downstream by the flow field. The negative vortex has cut off the connection between the lower shear layer and the positive vortex (Fig. 20b). The negative vortex is being shed while the positive one on the other side is reforming (Fig. 20c, f). The positive vortex draws the shear layer of opposite sign from the upper side of the wake across the wake centerline (Fig. 20d, g, h).

The vortex shedding frequencies are estimated from power spectra of the lift coefficients for periodic and symmetry boundary conditions. Figure 21a-d and 22a-d shows the power spectra for various side wall locations at $R_e = 100$ for periodic and symmetry boundary conditions, respectively. There is one prominent frequency in lift spectrum for all cases. The present results show that the vortex shedding frequency, in general, decreases with increasing side wall locations. The lift and drag coefficients exhibit a regular fluctuations in all cases. This is related to alternate vortex shedding. When side wall locations increase, the fluctuation magnitude decreases slightly. Comparing Fig. 23a with Fig. 23d for periodic boundary conditions, one can observe that the lift and drag coefficients decreases. The drag coefficient fluctuates at twice the frequency of the lift coefficient.

CONCLUSION

We have examined the influence of relaxation time parameter, upstream, downstream boundary locations and side wall locations using the Lattice Boltzmann simulations of incompressible. We found that the relaxation time parameters not only affect the physical quantities such as mean drag coefficients, root mean square value of lift coefficient and Strouhal number but also delay the vortex-shedding process and some of them are time consuming. We suggest $\tau = 0.526$ for flow around a square cylinder at $R_e = 100$. We further suggest that relaxation time parameter need to decrease for high Reynolds number flows. We have found there is an influence of upstream locations when brought near to the inlet boundary location the physical quantities reached to their maxima. Based on such observations, we found that at $L_1 = 15$ d LBM captures reasonable physical quantities and vortex shedding if the downstream is large enough. We also have found if the outlet boundary location is sufficiently large, i.e., $L_2 \geq 35$ dapproximately, the vortex-shedding is almost identical and the deviation between physical quantities such as mean drag coefficients, root mean square value of lift coefficient and Strouhal number are almost negligible. We have also observed that the side wall location play an important rule to study the vortex-shedding and physical quantities. We find that the side wall locations must need to locate approximately H = 10 dto avoid higher deviation between physical quantities and the vortex-shedding can easily goes further downstream. We observed that the periodic boundary condition results are slightly better than symmetric boundary condition. We found that the strength and size of the wake bubble are more appealing as they travel downstream in the form of alternating shed vortices for all examined cases. From this study it is found that the two-dimensional lattice Boltzmann method captures hydrodynamic forces and captures vortex shedding very well; if we have a suitable computational domain and a reasonable selection of relaxation time parameter τ. Most of the results in this study are compared with the experimental data and numerical results and present results are slightly better than experimental and some numerical results and are in better agreement with respect to other numerical results. These observations together with its easier implementation of LBM are a very useful alternative for practical flow computations.

ACKNOWLEDGMENT

The study describe in this research was supported by a grant from National Natural Science Foundation of China (Project No. 90715031). The financial support is gratefully acknowledged.

REFERENCES

Benard, H., 1926. On the frequency law of alternate eddies behind an obstacle. C.R. Acad. Sci., 182: 1375-1375.

Bendat, J.S. and A.G. Piersol, 1971. Random Data Analysis and Measurement Procedures. Wiley Interscience, New Jersey, ISBN: 0471317730.

Bhatnagar, P.L., E.P. Gross and M. Krook, 1954. A model for collision processes in gases, I. small amplitude processes in charged and neutral one-component system. Phys. Rev., 94: 511-525.

Chapman, S., T.G. Cowling and D. Burnett, 1970. The Mathematical Theory of Nonuniform Gases. 2nd Edn., Cambridge University Press, Cambridge.

Chen, H., S. Chen and W.H. Matthaeus, 1992. Recovery of the Navier-Stokes equations using a lattice-gas Boltzmann method. Phys. Rev. A, 45: R5339-5342.

Davis, R.W. and E.F. Moore, 1982. A numerical study of vortex shedding from rectangles. J. Fluid Mechanics, 116: 475-506.

Davis, R.W., E.F. Moore and L.P. Purtell, 1984. A numerical-experimental study of confined flow around rectangular cylinders. Phys. Fluids, 27: 46-59.

Dazhi, Y., M. Renwei, L.S. Luo and S. Wei, 2003. Viscous flow computations with the method of lattice Boltzmann equation. Prog. Aerospace Sci., 39: 329-367.

Fornberg, B., 1991. Steady incompressible flow past a row of circular cylinders. J. Fluid Mech., 225: 655-671.

Franke, R., W. Rodi and B. Schnung, 1990. Numerical calculation of laminar vortex shedding flow past cylinders. J. Wind Ind. Aerodynamics, 35: 237-257.

Frisch, U., N. Hasslacher and Y. Pomeau, 1986. Lattice-gas automata for the Navier-tokes equations. Phys. Rev. Lett., 56: 1505-1508.

Hassan, N., S.F. Anwar. and S. Sanghai, 2005. On the outflow boundary condition for external incompressible flows a new approach. J. Comput. Phys., 206: 661-683.

He, X. and L. S. Luo, 1997a. A priori derivation of the lattice Boltzmann equation. Phys. Rev. E, 55: R6333-R6336.

He, X. and L.S. Luo, 1997b. Theory of lattice Boltzmann method from the Boltzmann equation to the lattice Boltzmann equation. Phys. Rev. E, 56: 6811-6817.

Hollis, A., I. Halliday and C.M. Care, 2006. Enhanced mass-conserving closure scheme for lattice Boltzmann equation hydrodynamics. J. Phys. Math. Gen, 39: 10589-10601.

Ingham, D.B., T. Tang and B.R. Morton, 1990. Steady two-dimensional flow through a row of normal flat plates. J. Fluid Mech., 210: 281-302.

Kruger, T., F. Varnik and D. Raabe, 2009. Shear stress in lattice Boltzmann simulations. Phys. Rev. E, 79: 046704-046704.

Latt, J. and B. Chopard, 2008. Straight velocity boundaries in the lattice Boltzmann method. Phys. Rev. E, 77: 056703-056703.

Okajima, A., 1982. Strouhal numbers of rectangular cylinders. J. Fluid Mech., 123: 379-398.

Qian, Y.H., D. Dhumeieres and P. Lallemand, 1992. Lattice BGK models for Navier Stokes equation. Europhys Lett., 17: 479-484.

Shimizu, Y. and Y. Tanida, 1978. Fluid forces acting on cylinders of rectangular cross-section. Trans. Jsme. B, 44: 2699-2706.

Sohankar, A., C. Norberg and L. Davidson, 1996. A Numerical Study of Unsteady Two-Dimensional Flow Around Rectangular Cylinders at Incidence. Chalmers University of Technology-Gothenburg, Sweden.

Sohankar, A., C. Norberg. and L. Davidson, 1998. Low-Reynolds number flow around square cylinders at incidence study of blockage onset of vortex shedding and outlet boundary condition. Int. J. Numer. Methods Fluids, 26: 36-56.

Strouhal, V., 1878. On a particular way of tone generation. Wiedemann's Ann. Phys. Chem., 5: 216-216.

Succi, S., 2001. The Lattice Boltzmann Equation for Fluid Dynamics and Beyond. Oxford University Press, Oxford, ISBN: 0198503989.

Sukop, M.C. and D.T. Jr. Thorne, 2007. Lattice Boltzmann Modeling: An Introduction for Geoscientists and Engineers. 1st Edn., Springer, New York, ISBN-13: 978-3540279815.

Wolf-Gladrow, D.A., 2000. Lattice Gas Cellular Automata and Lattice Boltzmann Models: An Introduction. 1st Edn., Springer-Verlag, Berlin, ISBN-13: 978-3540669739.

Wolfram, S., 1986. Cellular automaton fluids 1 Basic theory. J. Statistical Phys., 45: 471-526.